CHALMERS
UNIVERSITY OF TECHNOLOGY

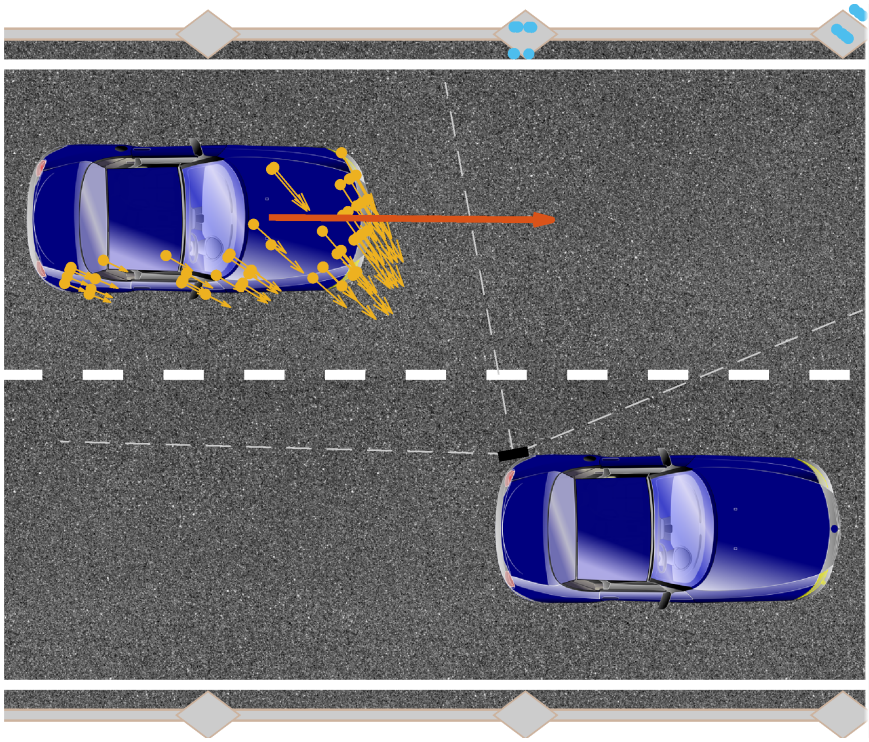

Target Identification Using Low Level Radar Measurements

Instantaneous Velocity Vector Estimation Using a Crude Angle Finding Algorithm and Clustering With an Automotive Radar

Master's thesis in System Control & Mechatronics

NICLAS CARLSTRÖM
ANTON ÖQVIST

Department of Electrical Engineering
CHALMERS UNIVERSITY OF TECHNOLOGY
Gothenburg, Sweden 2018

Master's thesis 2018:EX006

Target Identification Using Low Level Radar Measurements

Instantaneous Velocity Vector Estimation Using a Crude Angle Finding Algorithm and Clustering With an Automotive Radar

NICLAS CARLSTRÖM
ANTON ÖQVIST

CHALMERS
UNIVERSITY OF TECHNOLOGY

Department of Electrical Engineering
Division of System and Control
Chalmers University of Technology
Gothenburg, Sweden 2018

Target Identification Using Low Level Radar Measurements
Instantaneous Velocity Vector Estimation Using a Crude Angle Finding Algorithm and Clustering With an Automotive Radar
NICLAS CARLSTRÖM
ANTON ÖQVIST

Supervisor: Alexander Lyckell, Aptiv
Examiner: Tomas McKelvey, Department of Electrical Engineering

Master's Thesis 2018:EX006
Department of Electrical Engineering
Division of System and Control
Chalmers University of Technology
SE-412 96 Gothenburg
Telephone +46 31 772 1000

Cover: Visualisation of the doppler vectors of an overtaking vehicle with a plotted velocity relative ground and a heading relative the host car to which the radar is mounted.

Typeset in LaTeX
Gothenburg, Sweden 2018

Target Identification Using Low Level Radar Measurements
Instantaneous Velocity Vector Estimation Using a Crude Angle Finding Algorithm With an Automotive Radar
NICLAS CARLSTRÖM
ANTON ÖQVIST
Department of Electrical Engineering
Chalmers University of Technology

Abstract

This thesis investigates the possibilities of using a crude azimuth angle finding algorithm on every bin in the range doppler map from a mono pulse linear phase array radar. The crude angle finding algorithm used in this thesis requires low computing power and thus an azimuth angle is calculated for all measurements in the range doppler map. A grid based DBSCAN method was developed that has the potential of clustering together radar measurements from a single object based on range, doppler and the angle calculated by the crude angle finding algorithm. Furthermore a velocity vector containing the velocity and heading relative the host to which the radar is mounted is estimated using the clustered radar measurements for non-stationary objects. The methods have been verified by collecting data in a radar chamber, rigging scenarios and collecting data on an empty parking lot but also in ordinary traffic situations on roads in the proximity of Gothenburg, Sweden. The results show that the crude angle finding algorithm yields accurate results in the radar chamber where an angle sweep over the field of view of a corner reflector was made. (Some deviations from the true angle were found which are discussed further in the thesis.) Moreover the clustering is evaluated from the rigged scenarios where the cluster position is calculated using a developed algorithm and the velocity vector estimation of moving objects are compared to known velocities and headings from rigged scenarios using a test vehicle, a bicycle and a pedestrian travelling in the field of view. Results show that velocity vector estimation is possible for a vehicle and a bicycle under certain conditions.

Keywords: Radar, Angle Finding, Interferometry, DBSCAN, Clustering, Velocity Vector Estimation, Heading Estimation.

Acknowledgements

We would like to thank Aptiv for the opportunity and the support throughout this project. An extra big thank you goes to our supervisor **Alexander Lyckell** for his guidance and knowledge, **Andreas Andersson** for help with test driving and general support, **Honghui Yan**, **Tao Zhang** and **Konstantin Statnikov** for their ideas and inspiration and last but not least a big thanks to **Badeea Alazem**, **Sashi Praveen Kalli** and **Kamil Staszek** for their help with the radar chamber tests.

Niclas Carlström & Anton Öqvist, Gothenburg, February 2018

Contents

List of Figures

List of Tables

1

Introduction

1.1 Background

The automotive industry is currently in a phase where advanced active systems are being developed and implemented in vehicles to decrease the risks of accidents while driving. The terms 'autonomous' or 'self-driving cars' have during the last few years gained attention from media and have thus in extension made most people in the developed world aware that cars may not require a driver in a not too distant future. Even though no company as of today can claim that their cars are completely autonomous most companies have some degree of automation in their cars e.g. adaptive cruise control, automatic emergency braking and 'stay in lane assist'. Active systems like these require detailed measurements of the surrounding world to function properly and safely which is usually done by combining measurements from both cameras and radar units. Even though both cameras and radar units usually are being used it is of interest to isolate these sensors and examine ways to improve the performance of them individually and thus improve the final performance when both types of sensors are being used.

A typical radar sensor used in the automotive industry produce measurement data in two dimensional range doppler maps for each antenna. A range doppler map contains spectral information about the range and the radial velocity of the objects of which the transmitted wave was reflected against. If the radar sensor consists of multiple antennas the direction of the reflected waves can be estimated and thus yield a third dimension to the data from the radar sensor containing angular information about the objects that caused the reflections. However, as is more described in the theory Section, the measurement needs filtering and further processing before separate reflection points also called detections could be discriminated from the spectral data and reported to other units in the car. The processing power and available RAM is often limited due to financial reasons and it is therefore common that the maximum number of reported detections is limited. This requires ways of prioritising data that should be classified as detections or not. Furthermore, it is also common that the angle estimation is done once detections have been classified to save processing power and RAM which could make it hard to prioritise which detections that are most important and thus should be reported.

1.2 Purpose

The purpose of this thesis is to implement a low cost angle finding algorithm which could run on all data points in the range doppler map early on in the signal processing scheme. It will also be examined how this angle information can be used with clustering techniques to improve the understanding of the measured scenario by distinguishing data from different targets like guardrails, cars and bicycles and determine their position. The targets will be classified as moving or stationary by correcting the measurement with the motion of the host vehicle and estimating the full velocity vector of the target. All calculations will be done in one time sample and without filtering over time.
The benefit of having this kind of information in the signal processing scheme is that one could prioritise the measured data and make sure that the reported detections (peaks in the range doppler map) that is outputted from the radar comes from the important targets in the scenario, like cars moving towards the host vehicle. Radar trackers that filter detections over time could also benefit from instantaneous velocity vector measurement for each detection along with a grouping of detections that originates from the same physical target.

1.3 Scope

The scope is limited to post processing of already collected data, meaning that nothing was implemented to run in real time in an actual vehicle. However, data was collected both in a radar chamber where specific scenarios were set up and in a test vehicle where certain scenarios were staged but data was also collected from every day traffic scenarios. All data have been collected using a linear antenna array radar. No tracking, time filtering or fusion between radar units was done, meaning that all signal processing is done using data collected during one time sample and with one radar unit.

2
Theory

2.1 Radar Fundamentals

The core concept of a RADAR (**RA**dio **D**etection **A**nd **R**anging) unit is that it transmits an electromagnetic wave that propagates through space and when the wave reaches an object the wave reflects and propagates in the opposite direction back towards the radar unit that measures the reflected wave. The characteristic of the transmitted wave can be different depending on the purpose of the radar and the objects that are desired to be measured. Hence, there are several sub categories of radar systems using different methods to generate a desired waveform characteristic. The radar used in this thesis is of type LFMCW-RADAR where LFMCW stands for **L**inear **F**requency **M**odulated **C**ontinuous **W**ave. A LFMCW-RADAR generates the propagating wave by mixing a linear frequency sweep on top of a constant carrier frequency f_c. One full frequency sweep is called a chirp and the time it takes to perform one full sweep is called dwell time. A series of chirps are being transmitted during one measurement which in radar terminology is referred to as a frame. Furthermore, the frequency sweep from start to end is referred to as the bandwidth of the sweep [1]. A visualisation of the different concepts are presented in Figure 2.1 below.

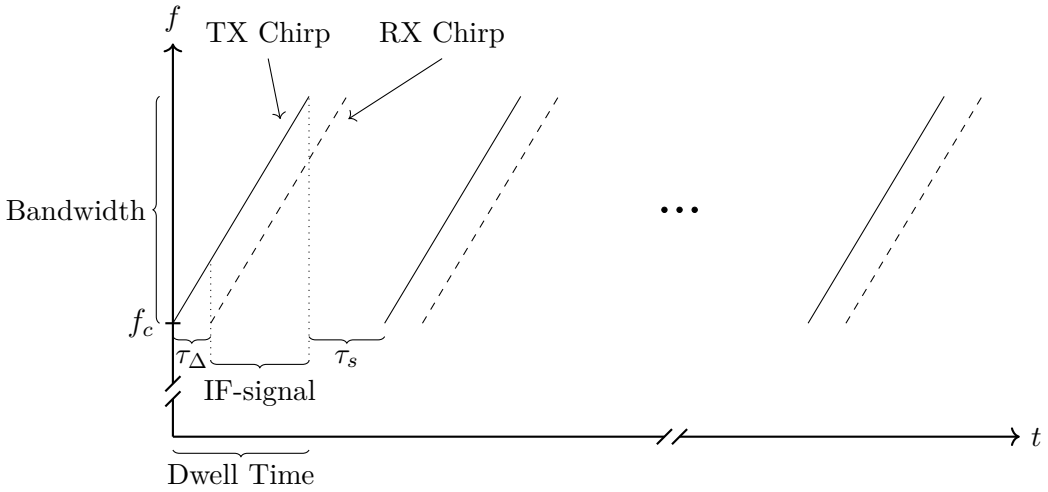

Figure 2.1: An illustration of the core concept in a radar measurement. The radar transmits and receives a chirp which is then mixed to create the IF-signal on which both the range FFT and doppler FFT is done

2.1.1 Range Measurements

A larger bandwidth impacts the range resolution and the maximum range depends on the dwell but also on how fast one samples the chirp. As the chirp is being transmitted on the carrier frequency the signal will reflect on objects within range of the radar and a replica of the chirp is received by the radar with some delay in time τ_Δ. By filtering out the carrier frequency and mixing the transmitted signal with the received signal one gets what is referred to as an IF-signal which stands for **I**ntermediate **F**requency. Since the reflection is an exact replica of the transmitted one the IF-signal is a new signal with a frequency and a phase shift equal to the difference between the instantaneous frequencies and the difference between the phase shifts of the transmitted and received signals. Since the chirps varies in frequency over time, reflections on objects at different distances from the radar will result in IF-signals with different frequencies and the distance to the objects can thus be calculated using the frequency of the specific IF-signal [1].

2.1.2 Range Rate Measurements

If an object is in motion the distance to the radar for every reflected chirp during one frame is different. However, the time between the chirps is very small and the difference in the IF-signals frequency for every chirp that arises from this small displacement in range is far smaller than the range resolution and will thus not yield a different range measurement between chirps. The phase difference of the IF-signals however is effected due to this small displacement of the moving object as is visualised in Figure 2.2. This is because the wavelength of the propagated wave is in the same order of magnitude as the expected small displacement in range of the moving object. The wavelength of the propagated wave, the phase difference between the IF-signals of each chirp and the time between the chirps can thus be used to determine the radial velocity of the object relative to the radar. There is a limit to the maximum radial velocity the radar can measure due to the fact that the phase of a sinusoidal wave is ambiguous. If the small displacement of a moving object between chirps is larger than half a wavelength of the propagated wave the resulting phase difference of the IF-signals is larger than π. This is thus ambiguous since phases larger than π are equal to negative phases smaller than $-\pi$. In a scenario like this the impact would be that the moving object is interpreted as moving towards the radar while in reality it is moving away from the radar. The maximum measurable radial velocity the radar is thus a function of the propagated waves' wavelength and the time between the chirps.
The analogue IF-signal is low pass filtered and digitalised through an ADC and then passed to the digital signal processing unit. A fast Fourier transform (FFT) over the IF-signals for each chirp generates magnitude peaks at the frequencies in the IF-signal which directly corresponds to a range of a measured object. Another FFT is then done over the phases of the range FFT which yields magnitude peaks at the phase shifts of the IF-signals which directly corresponds to the radial velocity of the object at the corresponding range. The result from the two FFTs can thus be represented as magnitudes in a two dimensional matrix, often referred to as the range doppler map, as shown in Figure 2.3. Objects within the field of view of

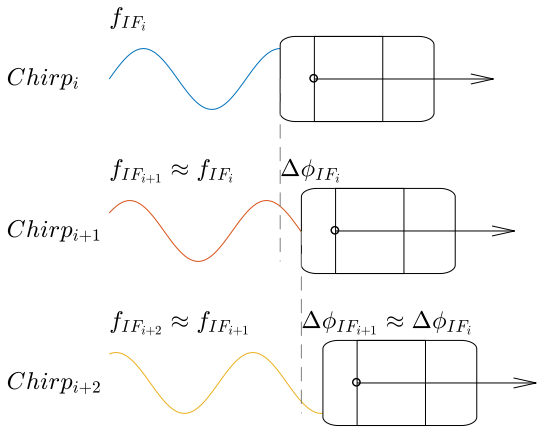

Figure 2.2: Illustration of the IF-signal for a moving object. The small displacement in range between chirps does not affect the IF-signals frequency in practise. The phase shifts between chirps are affected and are used to measure the radial velocity of the object

the radar show up as islands of varying size in the range doppler map. Since the frequency resolution of a FFT is limited to the number of samples that are being transformed these islands most often span over several bin pairs in the range doppler map. The actual range and radial velocity is calculated by multiplying the bin pairs with their corresponding resolution [1].

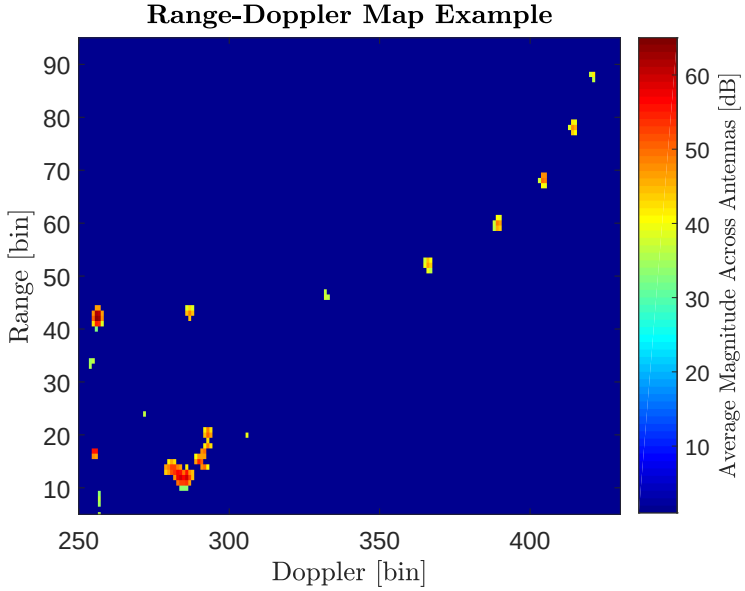

Figure 2.3: An example of how a range doppler map may look for one measurement. Magnitude is averaged across the antennas and marked with colours

2.1.3 Angle Measurements

In the previous parts it is mentioned that chirps are being transmitted and received which is done using at least one transmitting and one receiving antenna. For linear phase array radars multiple antennas are mounted in rows and columns with some spacing apart. An important term when discussing angle estimation of radar detections is what is referred to as the boresight of the radar. The boresight is defined as an orthogonal vector to the plane where the array of antennas is mounted and is located in the centre of the rows and columns of the antennas. Measurements from antennas in rows can be used to measure the angle in the horizontal plane of objects relative to the boresight of the radar. This angle is referred to as the azimuth angle in radar terminology. Similarly, the measurements from antennas in columns are used to measure the angle in the vertical plane of objects relative to the boresight of the radar and this angle is referred to as the elevation angle in radar terminology. A visualisation of the boresight vector, azimuth and elevation angle is presented in Figure 2.4. Furthermore, for every receiving antenna the two FFTs described above are performed and thus another range doppler map is generated. One could visualise this by placing the range doppler maps on top of each other creating a box of data that is as high as the number of antennas.

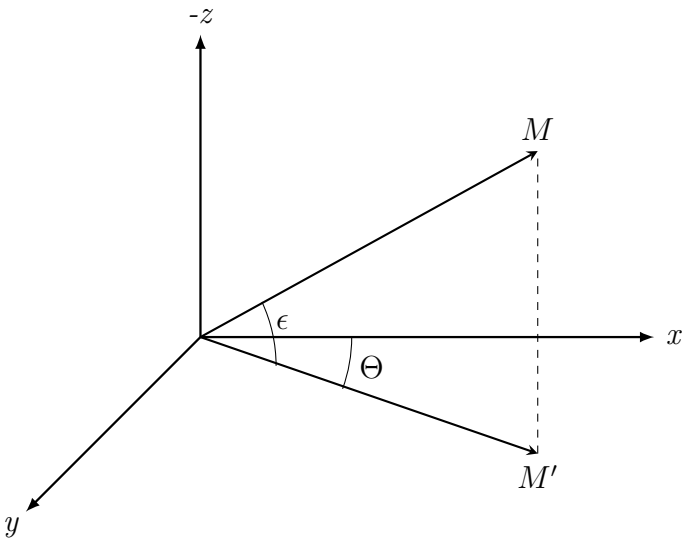

Figure 2.4: Definition of the boresight vector and the azimuth, θ, and elevation angle, ϵ. The boresight angle is defined along the x axis, M represents the vector to an arbitrary target and M' is the projection of M in the xy plane

As a reflected chirp of an object propagates back towards the radar it will reach the antennas at the same time given that the object is straight ahead of the radar. The object is in this example said to be in the boresight of the radar and have an azimuth angle of zero degrees. However, if the object is not in the boresight of the radar the reflected chirp that propagates back towards the radar will reach the antennas with some delay which gives rise to a different measured phase at each antenna $\Delta\phi$. This phase difference $\Delta\phi$ thus contains information of the azimuth angle to a measured object as is illustrated in Figure 2.5. It is common to compress the range doppler

maps in to one for each antenna by taking the mean of the magnitudes for each bin pair while keeping the phase difference between the antennas to make an azimuth angle estimation. The azimuth angle of the reflected wave can thus be calculated as

$$\theta = \sin^{-1}\left(\frac{\lambda}{2\pi d}(\Delta\phi + 2\pi n)\right) \tag{2.1}$$

where λ is the wavelength of the propagated wave, θ is the azimuth angle and d is the distance between the antennas. The term $2\pi n$ describes the unambiguities of a sine function with n number of periods.
By the same reasoning as for the maximum measurable radial velocity, unambiguous angle results are only possible if the distance between the antennas is equal to or less than half a wavelength λ [1, 2]. A bin pair of range and doppler along with its azimuth angle is referred to as a bin measurement or BM for short throughout the report.

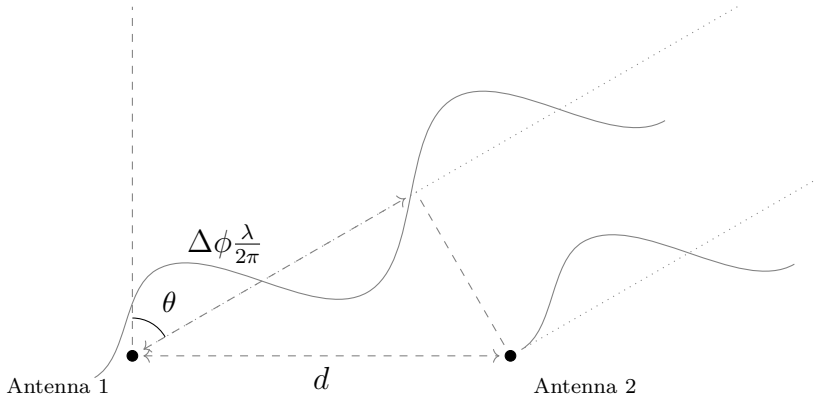

Figure 2.5: A visualisation of the principle behind calculating the angle to an object

2.2 Scatterers and Detections

The range doppler map holds as explained information about the range and radial velocity of the signal measured by each antenna. Since the signal reflected against a target will have reflection points spread out over the surface of the object it will be shown as an island distributed over different ranges and radial velocities. The magnitude of the signal response from a certain bin in the range doppler map will therefore be a measure of how much energy the reflections contain of this particular range and doppler bin. Peaks in the range doppler map will thus correspond to centres of areas on a target where the signal reflected against, also called scatter points or scatterers.
A full set of range doppler maps from each antenna is not a convenient format to output from the sensor. Firstly since it is simply too much data and secondly because most of the data in the range doppler map is just filtered out as noise since only a fraction of all ranges and radial velocities will be represented in one measurement. Instead only a few key points in the range doppler map could be outputted from the

sensor. These points are normally referred to as detections in radar terminology. There are multiple ways of choosing detections but it is common that the peaks of the range doppler map is sorted out since they are the scatter points with highest signal strength. But even so a scenario with a lot of targets may produce too much data to output and therefore only the peaks that are considered most important are outputted. It is also common that the angular information only is calculated on the peaks that are to be reported as detection to save processing power and RAM which could make it even harder to determine which detections that best describe the measured scenario.

2.3 Host Induced Velocity

If the radar is mounted on a vehicle the vehicle is called a host. As the host is moving the radar will thus move along with it. This movement does not affect the range measurements since the propagated wave travels significantly faster than the host. The radial velocity measurements of objects however is strongly affected by the host induced movement since the phase shift is sensitive to small changes in range as described in the previous Section. In practise this have the effect that objects which are stationary will have a measured radial velocity inherited by the movement of the host. By the same reasoning another vehicle which keeps the same velocity as the host relative to the radar will measure zero radial velocity. The movement of the radar caused by the movement of the host must thus be compensated for as it is desired to measure radial velocities relative to the ground and not to the host itself to be able to determine whether an object is stationary or in motion. Depending on the velocity and the orientation of the radar in relation to the host one can form what is called a velocity profile over azimuth angle [3]. The velocity profile thus describes the expected measurements in radial velocity induced by the movement of the host over the field of view of the radar.

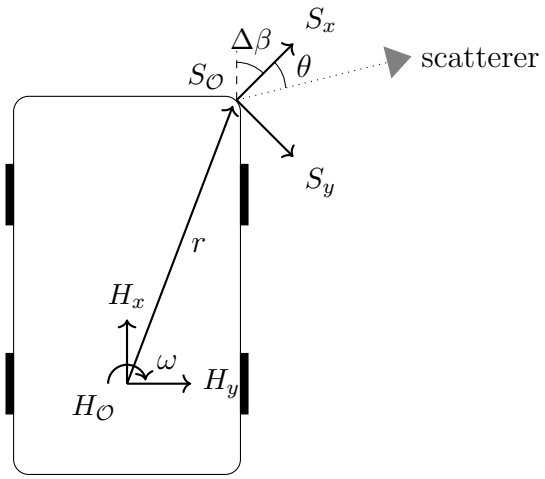

Figure 2.6: An illustration of how the radar may be positioned relative the host coordinate system

The host coordinate system is defined according to SAE J670-200801 standard for coordinate systems of road vehicles. This means that the origin, $H_{\mathcal{O}}$, of the coordinate system centred in the vehicles rear axis with x-axis pointing forward in the direction of the vehicle, y-axis to the right and z-axis pointing down in the ground [4]. The location and orientation of a radar mounted on the host can thus be defined using another coordinate system, $S_{\mathcal{O}}$, with origin and orientation relative to the host coordinate system $H_{\mathcal{O}}$. The boresight of the radar is aligned with the x-axis of $S_{\mathcal{O}}$. See Figure 2.6 for reference.
The velocity of the origin point $S_{\mathcal{O}}$ consists of velocity vectors from the host forward velocity but also from the turning rate of the host. As the host is turning the sensor will move in an arch trajectory with a radius r, where r is the distance to the radar sensor coordinate system $S_{\mathcal{O}}$ relative the host coordinate system $H_{\mathcal{O}}$. The tangential velocity of a point at $\boldsymbol{r}$ can be described using the cross product of the rotational velocity $\boldsymbol{\omega}$ vector and the position vector of the point $\boldsymbol{r}$ [5]. Since the turning rate is strictly around the z-axis the solution to finding the tangential velocity, $\boldsymbol{v}_{\perp}$, in the origin point $S_{\mathcal{O}}$ reduces to two dimensions as in Equation (2.2). Where $\boldsymbol{r}$ is the position vector of the point and ω is the turning rate of the host. Equation (2.2) thus describes the velocity in the arch trajectory induced by the turning rate of the host expressed in the host coordinate system $H_{\mathcal{O}}$.

$$\boldsymbol{v}_{\perp} = \boldsymbol{\omega} \times \boldsymbol{r} = \begin{bmatrix} v_{\perp_x} \\ v_{\perp_y} \\ v_{\perp_z} \end{bmatrix} = \omega \begin{bmatrix} -r_y \\ r_x \\ 0 \end{bmatrix} \tag{2.2}$$

The forward motion of the host must then be added to the total velocity of the sensor as

$$\boldsymbol{v}_S = \begin{bmatrix} v_{S_x} \\ v_{S_y} \end{bmatrix} = \begin{bmatrix} v_{H_x} \\ 0 \end{bmatrix} + \begin{bmatrix} v_{\perp_x} \\ v_{\perp_y} \end{bmatrix}. \tag{2.3}$$

The direction of the induced velocity on the radar can be described as the angle between its velocities in x and y direction. The orientation of the radar relative to the host, $\Delta\beta$, must be taken in to account to relate the induced velocity expressed in the host coordinate system $H_{\mathcal{O}}$ to the radial velocities that is measured in the radar's coordinate system $S_{\mathcal{O}}$. The direction of the induced velocity on the radar expressed in the radar's coordinate system $S_{\mathcal{O}}$ can thus be calculated as

$$\alpha_S = \tan^{-1}\left(\frac{v_{S_y}}{v_{S_x}}\right) - \Delta\beta. \tag{2.4}$$

The final expression to describe the by the host induced measured radial velocity, v_r, at an arbitrary azimuth angle, θ, within the field of view of the radar can be expressed as

$$v_r(\theta) = -|\boldsymbol{v}_S| \cos(\theta - \alpha_S). \tag{2.5}$$

2.4 Heading and Velocity of Non-Stationary Objects

As mentioned in the Section 2.1 the velocity of objects that causes a reflection is measured radially relative to the radar. This means that the radar is only able to measure the total velocity of an object if the object moves radially directly towards or away from the radar. If the object however moves in any other direction only a part of the objects total velocity is measured by the radar. The direction of the movement is commonly referred to as an objects heading. Considering a scenario where a small object is in the boresight of a stationary radar and is moving directly towards the radar. In such scenario the total velocity of the object is in radial direction to the radar and the total velocity of the object is thus measurable. However, considering the same scenario except now the object moves perpendicular to the radar. In this case the radar would measure zero velocity of the object since the object neither moves towards or away from the radar. For a moving point at an azimuth angle θ relative the radar its full actual velocity is measurable only if its heading, α, is equal to θ and none of the actual velocity is measurable if the heading α is perpendicular to θ.
Assuming though that moving objects are large enough to yield several reflections from different points on the object the velocity measurements from these bin measurements can be used to estimate an objects velocity profile [6].

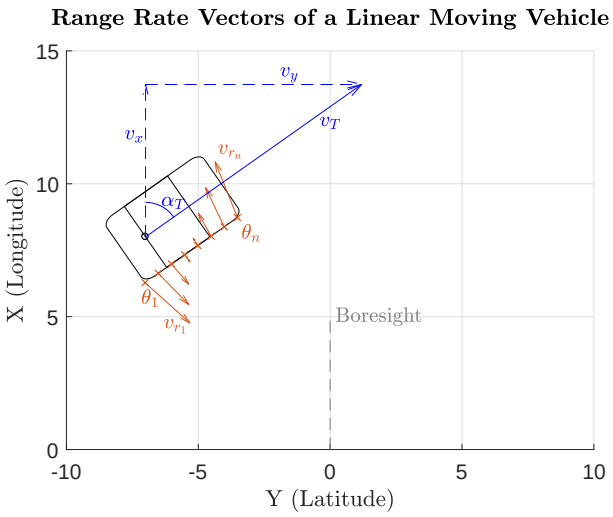

Figure 2.7: Illustration of the measured range rate vectors of a moving vehicle where v_T is the velocity of the vehicle and α_T is the heading relative the boresight of the radar

Figure 2.7 illustrates how the velocity measurements from several bin measurements on a vehicle would look like if all the reflections was reflected on the side of the vehicle. By assuming that the vehicle causing the reflections is travelling in a linear motion the total velocity vector V_T of all the reflections have the same direction. However, since the reflections originates from different points on the vehicle the measured radial velocity, v_r, is a function of the azimuth angle, θ, to the point of

the reflection. Assuming that N number of bin measurements from the moving vehicle have been received by the radar the radial velocity can be expressed as

$$\begin{bmatrix} v_{r_1} \\ v_{r_2} \\ \vdots \\ v_{r_N} \end{bmatrix} = \begin{bmatrix} cos(\theta_1) & sin(\theta_1) \\ cos(\theta_2) & sin(\theta_2) \\ \vdots & \vdots \\ cos(\theta_N) & sin(\theta_N) \end{bmatrix} \begin{bmatrix} v_x \\ v_y \end{bmatrix}. \tag{2.6}$$

Equation (2.6) is an over determined system if it consists of more than two reflected bin measurements on the moving object which can be solved using a variety of different regression techniques. By expressing the velocities v_x and v_y as the vehicles speed, v_T, and heading, α_T, as

$$v_x = v_T cos(\alpha_T) \ , \ v_y = v_T sin(\alpha_T), \tag{2.7}$$

the expression for the measured radial velocity at a certain azimuth angle becomes

$$v_{r_i} = v_T(cos(\theta_i)cos(\alpha_T) + sin(\theta_i)sin(\alpha_T)). \tag{2.8}$$

By using the trigonometric identities

$$cos(a)cos(b) = \frac{1}{2}(cos(a-b) + cos(a+b)) \tag{2.9}$$

$$sin(a)sin(b) = \frac{1}{2}(cos(a-b) - cos(a+b)) \tag{2.10}$$

the expression for the measured radial velocity reduces to

$$v_{r_i} = v_T cos(\theta_i - \alpha_T). \tag{2.11}$$

The heading of a moving object is thus equal to the negative phase shift of the objects velocity profile. As can be seen from Equation (2.11) the derived expression is very similar to the expression in (2.5) which describes the velocity profile for the radar due to movement of the radars host. This is because the two expressions essentially describe the same thing, namely how velocity measurements are dependent on the azimuth angle of objects and the heading and the velocity of an object or the radar itself. The radar would yield the same velocity measurement if an object is moving towards a stationary radar at a certain angle and velocity as a radar on a moving host that approaches a stationary object with the same velocity and angle. To estimate a moving objects heading and velocity relative to the host one must first compensate the radial velocity measurement induced by the host on the radar. The over determined system in (2.6) then becomes

$$\begin{bmatrix} v_{r_1} + v_S cos(\theta_1 - \alpha_S) \\ v_{r_2} + v_S cos(\theta_2 - \alpha_S) \\ \vdots \\ v_{r_N} + v_S cos(\theta_N - \alpha_S) \end{bmatrix} = \begin{bmatrix} cos(\theta_1) & sin(\theta_1) \\ cos(\theta_2) & sin(\theta_2) \\ \vdots & \vdots \\ cos(\theta_N) & sin(\theta_N) \end{bmatrix} \begin{bmatrix} v_x \\ v_y \end{bmatrix}. \tag{2.12}$$

The parameters of Equation (2.11) can then be calculated where the velocity of the object is found using Pythagoras theorem

$$v_T = \sqrt{v_x^2 + v_y^2}. \tag{2.13}$$

The heading angle is calculated using Equation (2.14) where the offset mounting angle, $\Delta\beta$, of the radar on the host is accounted for.

$$\alpha_T = tan^{-1}\left(\frac{v_y}{v_x}\right) + \Delta\beta \tag{2.14}$$

3
Methods

3.1 Crude Angle Finding

The crude angle finding algorithm must be very computational efficient for it to be possible to run in real time on all bin measurements in the range-doppler map but still produce a fairly good result so that the measured scenario could be accurately described. The crude angle finding algorithm therefore utilises a simple phase comparison between antennas as described in (2.1) but uses two antenna pairs to enhance the accuracy of the angle.

3.1.1 Antenna Array

The radar used in this thesis has a linear antenna array of horizontally aligned antennas and the crude angle finding algorithm uses three of them which are distributed according to the Figure 3.1. Since only horizontal antennas are used the elevation angle is not calculated.

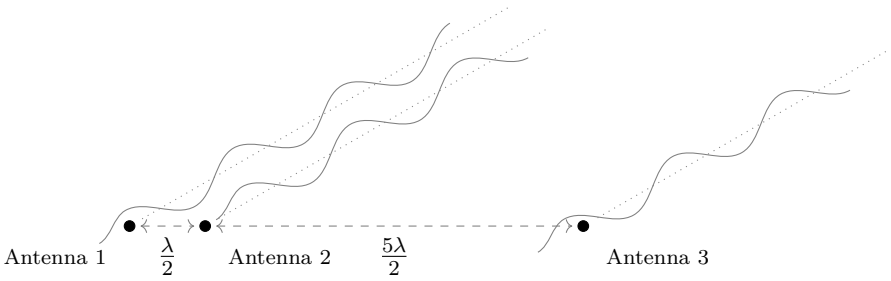

Figure 3.1: Antenna array description

By using the Equation (2.1) the azimuth angle of a point in the range-doppler map can be calculated with the phase difference over the first two antennas as

$$\theta = \sin^{-1}\left(\frac{\Delta\phi}{\pi} + 2n\right) \tag{3.1}$$

since the distance d between the antennas are $\frac{\lambda}{2}$ where λ is the wavelength of the transmitted radar signal. This means that there can only be one unique result of θ for a phase difference between $-180°$ and $180°$ as only $n = 0$ produces an argument between -1 and 1. When the phase difference between the second and the third

antenna is used to calculate the azimuth the wider distance ($d = \frac{5\lambda}{2}$) produce an ambiguous result since the Equation (2.1) instead becomes

$$\theta = \sin^{-1}\left(\frac{\Delta\phi}{5\pi} + \frac{2n}{5}\right). \tag{3.2}$$

Here $n = -2, -1, 0, 1$ and 2, all produce valid results and for every phase difference and thus 5 different azimuth angles are possible.
The advantage of using the wider antenna pair is however that the measurement is more accurate because a change in phase difference produces a smaller change in azimuth. In Figure 3.2 the resulting azimuth error is plotted over the phase difference when an constant error ϵ is applied to the measured phase difference between both the narrow and the wide antenna pair. It can clearly be seen that the narrow antenna pair is more sensitive to this disturbance.

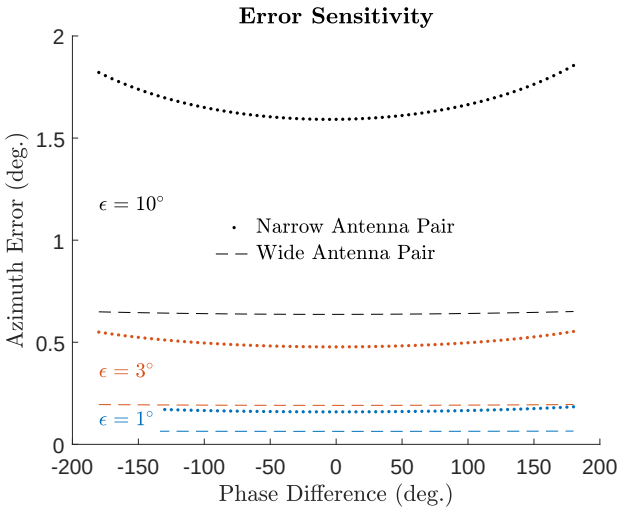

Figure 3.2: Error sensitivity of the phase comparison technique for the two antenna pairs

In order to produce a high accuracy without ambiguities the narrow antenna pair could be used to dissolve ambiguities in the measurement from the wide antenna pair. This comes with a risk that the algorithm chooses the wrong azimuth angle from the ambiguities which would produce an high error. If the phase difference, $\Delta\phi$, is 180° and the wrong azimuth from the wide antenna pair is chosen the algorithm will produce one of the following errors in azimuth:

$$\begin{aligned} \sin^{-1}\left(\frac{1}{5}\right) - \sin^{-1}\left(-\frac{1}{5}\right) &\approx 23° \\ \sin^{-1}\left(\frac{3}{5}\right) - \sin^{-1}\left(\frac{1}{5}\right) &\approx 25° \\ \sin^{-1}(1) - \sin^{-1}\left(\frac{3}{5}\right) &\approx 53°. \end{aligned} \tag{3.3}$$

Another risk is that when a target is close to the outer edge of the field of view the phase could potentially be measured as −180° instead of 180° and the other way

around. The algorithm will then have 5 possible solutions that have the following errors

$$\begin{aligned}
\sin^{-1}\left(-\frac{3}{5}\right) - (-90) &\approx 53^\circ \\
\sin^{-1}\left(-\frac{1}{5}\right) - (-90) &\approx 78^\circ \\
\sin^{-1}\left(\frac{1}{5}\right) - (-90) &\approx 102^\circ \\
\sin^{-1}\left(\frac{3}{5}\right) - (-90) &\approx 127^\circ \\
\sin^{-1}(1) - (-90) &= 180^\circ.
\end{aligned} \tag{3.4}$$

3.1.2 Calibration

The result of the measured phase differences for different azimuth angles depends on the performance of the electrical components, length of physical wires and other properties that are specific to each radar unit. In order to keep a high performance in the crude angle finding and keep a persisting performance over multiple units a unit specific calibration is needed. This is done by measuring the phase difference between antennas for the two antenna pairs for targets at different azimuth angle. A look up table (LUT) is created for each radar unit and antenna pair and can later be used to easily transform the measured phase difference to azimuth angle and keep a good performance on all radar units.

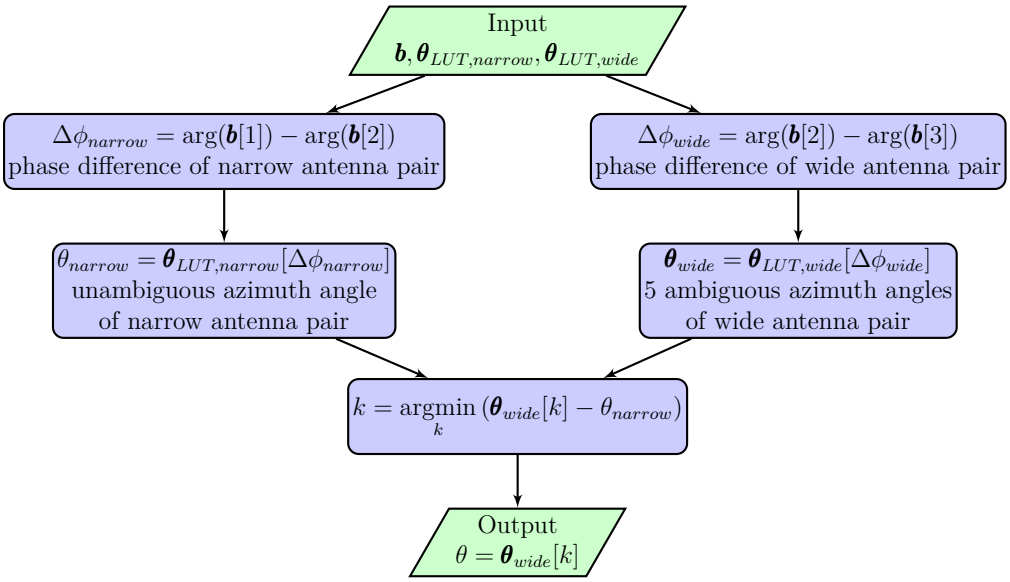

Figure 3.3: Flowchart describing the crude angle finding algorithm

3.1.3 Crude Angle Finding Algorithm

Figure 3.3 shows a flowchart of how the crude angle finding algorithm was implemented. The symbol $\boldsymbol{b}$ represents a calibrated bin measurement of a range-doppler bin, $\boldsymbol{\theta}_{LUT,wide}$ is the look up table between phase difference and azimuth for the wide antenna pair, $\boldsymbol{\theta}_{LUT,narrow}$ is the look up table for the narrow antenna pair, θ is the resulting azimuth.

3.2 Velocity Profile

As mentioned in Section 2.3 the movement of the host that acts upon the radar needs to be compensated for to get radial velocity measurements relative to the ground and not relative to the host. In Figure 3.4 one can see the impact of the host movement induced on the measurements from the radar. In this Figure the doppler measurement has not been compensated with the velocity profile of the radar but the velocity profile over the entire field of view have been plotted along with all the doppler measurements at this time instance. At this time instance the host is travelling at a speed of roughly 8.3 m/s and is slightly turning to the right at a yaw rate of about 5 degrees/s and the radar is mounted at the front right of the host with an offset angle of 60 degrees. Only stationary objects are within the field of view except for an oncoming car in the edge of the field of view of the radar.

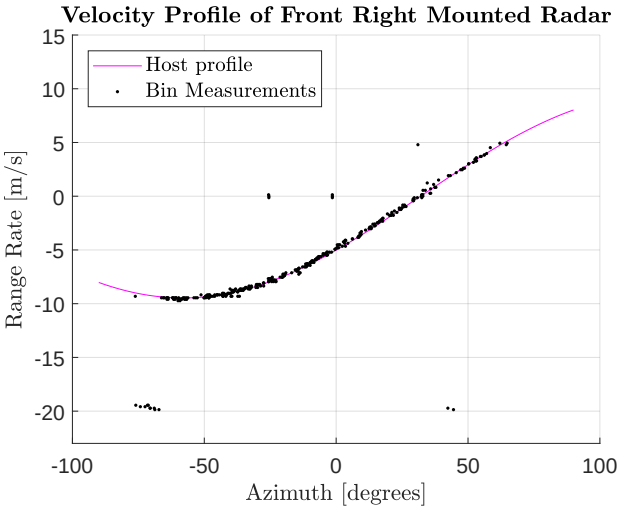

Figure 3.4: Illustration of how the velocity profile of the radar varies over azimuth angle to the object that caused the reflection. The compensated doppler is thus a function of the azimuth angle

Figure 3.4 illustrates the induced velocity profile of the radar due to the movement of the host. The velocity of an oncoming car is measured as roughly double its absolute velocity since host keeps roughly the same velocity in opposite direction and stationary objects have a measured relative velocity dependent on the azimuth angle to the object. The doppler vectors are thus compensated with the velocity profile as

$$d_{comp}(\theta) = d_{raw} + v_S \cos(\theta - \alpha_S). \tag{3.5}$$

3.3 Clustering

In order to separate the range-doppler-azimuth data into different targets the data needs to be grouped together with a clustering algorithm. The assumption is that the reflected energy from a target, like for example a car, bicycle, pedestrian or guard rail will have similar properties and that it thereby can be separated from the rest of the data. One advantage of having the crude azimuth this early on in the signal processing scheme is therefore that this kind of clustering can be done more accurately. Different objects in the scene can have very similar range and doppler even though they originate from totally different positions relative to the host vehicle and an estimation of the azimuth angle could therefore help in clustering objects with similar properties together. An example of a measurement on a highway road is shown in Figure 3.5. The range-doppler-azimuth map shows multiple islands corresponding to an overtaking car and the poles of a guardrail. The car can be seen to have similar range and doppler values and are spread out in azimuth since the radar get reflections along the side of the car. The white areas are range-doppler areas where it is estimated that only noise has been measured.

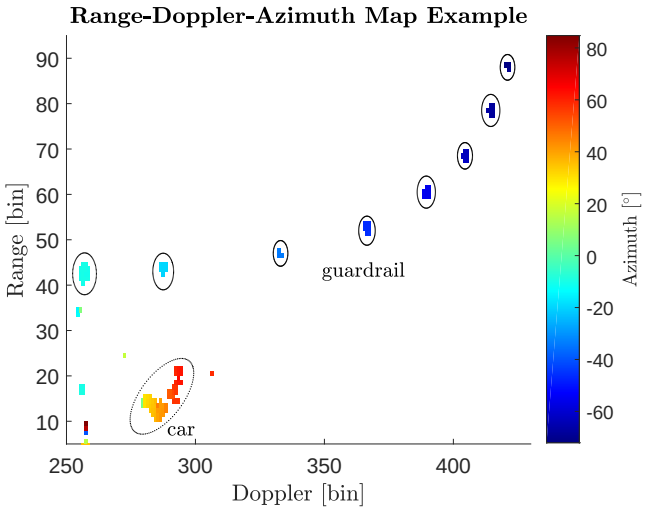

Figure 3.5: Example of range-doppler-azimuth map from a scenario with an overtaking car close to a guardrail. The car and guardrail poles show up as small islands on range and doppler bins corresponding to their range and radial velocity to the radar. Azimuth angle are marked with increasing colours from blue to red

3.3.1 DBSCAN

DBSCAN is a commonly used clustering algorithm for spatial data and has the advantages that it does not require any particular knowledge about the scenario the data represents except for the density a target has in the range-doppler-azimuth map. Arbitrary number of objects could be handled and the shapes of the clusters does not matter [7]. This is important since the object in an automotive scenario may look very different dependent on their shape, pose and movement, but also the host vehicle motion has a big impact on how other objects will look in the range-doppler-azimuth map.

The principle behind DBSCAN is that a data point is classified as part of a cluster with the points that surrounds it if the density around it is high enough. This is in practise implemented with 3 parameters: the minimum amount of neighbouring points (*minPts*), a distance describing the size of the neighbourhood (*eps*) and a distance function used to calculate the neighbourhood of a point. For each point in the data the number of neighbours within the distance of *eps* is calculated using the distance function. If the amount is higher than *minPts* the density is high enough and the point is considered to be a core point in a cluster together with its neighbouring points. Clusters can besides core points also have border points that are points that have a core point in its neighbourhood but lack the density within it to be a core point. Points in the data set that are neither a core nor a border point does not belong to any cluster and is considered noise. An example is shown in Figure 3.6 where the minimum amount of neighbouring points within the neighbourhood is two. Red points are therefore considered core points, blue border points and black is noise.

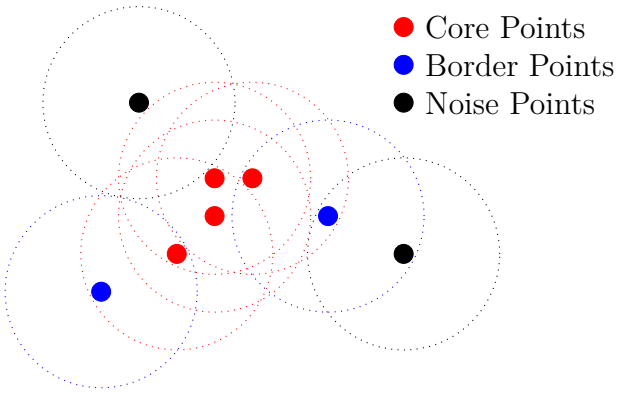

Figure 3.6: Example of a clustered data set with minimum number of points in neighbourhood equal to three. The red points all have two or more number of neighbours in their neighbourhood (marked with a circle) and are therefore core points. Blue points have a core point in their neighbourhood and are therefore border points. Black points is noise since they do not have any core points in their neighbourhood

3.3.2 Grid Based Implementation

The range-doppler-azimuth map can be saved as a matrix where the range and doppler bin corresponds to the position in the matrix and each value is the azimuth angle for that specific bin measurement in the range-doppler map. This enables a very fast grid based implementation of DBSCAN where the neighbourhood can be directly defined by *eps*. *eps* is defined as a three dimensional vector where two values describe the size of a neighbourhood as a range-doppler kernel and the third is an azimuth tolerance. In order to calculate the number of neighbours to a point now all the algorithm has to do is to extract all azimuth values in the matrix that are *eps*[1] and *eps*[2] rows and columns away from the point and count how many that are within *eps*[3] angle units. The benefit is that the number of distances that needs to be calculated for each point is significantly decreased compared to if *eps* were a euclidean distance and the ordering of the data did not have a spatial meaning. An example is shown in Figure 3.7 where the neighbours of the point with azimuth 10° is calculated and marked with red. In the left image the range-doppler kernel described by *eps* is shown as a red dotted square and all points within this kernel that have an azimuth value within 5° is considered neighbours. The right image instead show how the distance to all other points needs to be calculated with the distance function in order to count how many there are within the *eps*-distance from the point. In this example the clustering give the same result but the grid cluster have much lower complexity.

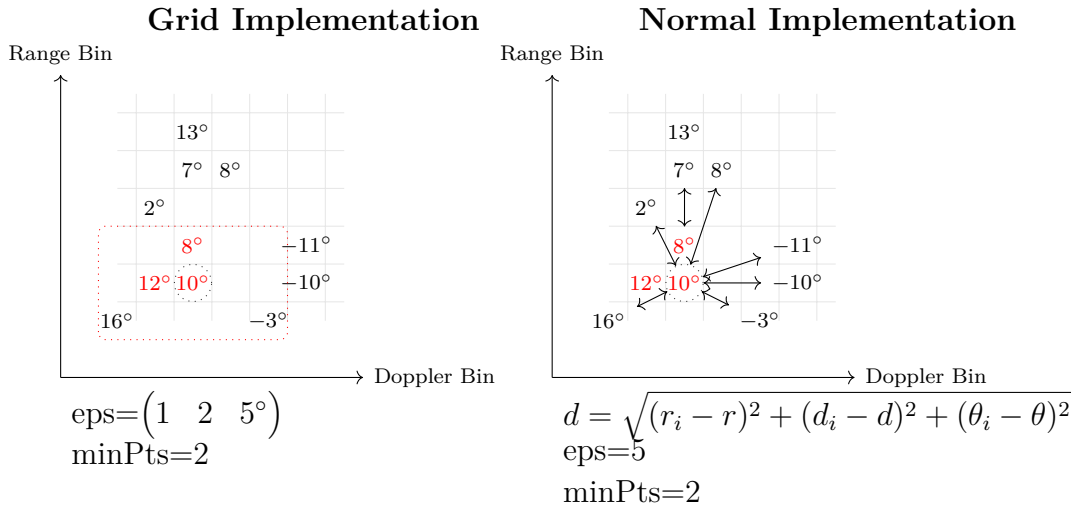

Figure 3.7: A illustration of counting the neighbour with the grid implementation of DBSCAN (left) compared to a general implementation of DBSCAN (right) where the data is not structured in spatially meaningful way. In the general implementation the distances to all points need to be calculated and compared to the *eps* while in the grid implementation only the closest values in the matrix need to be compared to the point

3.3.3 DBSCAN Flowchart

Figure 3.8 shows a flowchart describing the full clustering algorithm. The symbol θ_{map} denotes the azimuth map, *eps* the neighbourhood size where the first value is the size in range, second in doppler and the third in azimuth. The minimum number of points in a neighbourhood for it to have high enough density is denoted $minPts$. More detail on the implementation with pseudocode can be found in Appendix A.1.

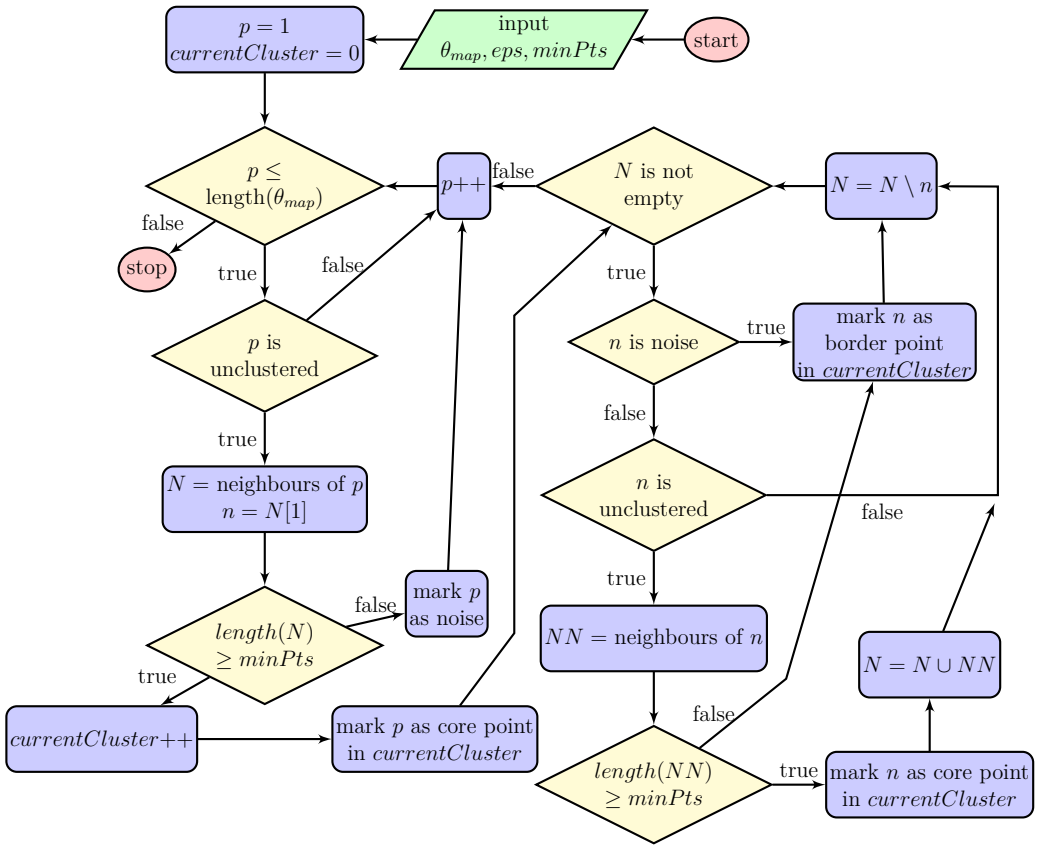

Figure 3.8: Flowchart describing the DBSCAN algorithm. Capital letters represent sets of points while lower case letters represent a point

3.4 Calculating Cluster Properties

Apart from the data in the range-doppler-azimuth map some additional information about each cluster is needed so that the importance of them can be determined. Each cluster must also have the following properties:

- range of the cluster centre
- doppler value of the cluster centre
- azimuth angle of the cluster centre
- classification of whether the cluster is stationary or moving
- estimated velocity vector of non-stationary clusters

3.4.1 Range and Doppler Position of Cluster Centre

A radar scatterer results in a peak that is spread out over multiple bins in the range-doppler-map and will therefore result in multiple bin measurements where, in an ideal case and only one point of reflection, the one with the highest magnitude is the centre. Bin measurements around this centre point of the scatterer have slightly different range and doppler values and the scatterers will therefore spread out in the range-doppler map. When calculating the range-doppler position of the cluster it is therefore necessary to use the magnitude of the bin measurements since a high magnitude indicates that a bin measurement belongs to a scatter centre.
The range and doppler value of the cluster is therefore calculated as a magnitude weighted average over all bin measurements in the cluster as

$$\begin{aligned} r_c &= \sum_{i=1}^{n} \frac{|\boldsymbol{b}_i|}{N_b} r_i \\ d_c &= \sum_{i=1}^{n} \frac{|\boldsymbol{b}_i|}{N_b} d_i \\ \text{where} \quad N_b &= \sum_{i=1}^{n} |\boldsymbol{b}_i| \\ \text{and} \quad n &= \text{number of bin measurements in cluster.} \end{aligned} \tag{3.6}$$

3.4.2 Azimuth Angle of Cluster Centre

The azimuth of the cluster is calculated differently since it is expected that a cluster can be built up by many scatters that are spread out along a line in the scenario. The result will be that there are groups with bin measurements around each scatter with similar azimuth but that these groups will differ in azimuth quite a lot between each other. Imagine for example a guardrail along the road. It will be built up by many different scatters with increasing range and azimuth that is spread out over the field of view. The cluster azimuth is therefore calculated as the maximum peak of a histogram over the azimuth angles which in practice will be the most frequent azimuth angle of the bin measurements in the cluster.

$$\begin{aligned} &\theta_c = \theta_k \quad \text{where} \\ &k = \underset{i}{\text{argmax}}(h_i), \quad i = 1, ..., K \quad \text{and} \\ &h_i = \sum_j \theta_j \quad \text{where} \\ &\theta_j \in \left\{ \theta_{min} + (i-1)\frac{\theta_{max} - \theta_{min}}{K} \leq \theta \leq \theta_{min} + i\frac{\theta_{max} - \theta_{min}}{K} \right\} \end{aligned} \tag{3.7}$$

Here $\boldsymbol{\theta}$ is the vector of all azimuth angles of the bin measurements in the cluster, $\theta_{min}/\theta_{max}$ is the minimum/maximum values of the azimuth vector, $\boldsymbol{h}$ is the histogram and K is the number of bins in the histogram.

3.4.3 Stationary/Moving classification

A simple way to determine whether a cluster is stationary, moving towards or away from the host would be to investigate the doppler value of the bin measurements relative to ground described in (3.5). If all of them are positive the cluster is moving away and if they are negative it is moving towards the radar. Values close to zero would then indicate that the cluster is stationary. However this is not at all true in all scenarios. As mentioned in the Section 2.4 bin measurements that are at an angle θ and have a heading perpendicular to θ will measure zero radial velocity. In practise this means that objects that actually are moving seems to be stationary from the radars point of view at a first glance. An example of a scenario is presented in Figure 3.9 where a vehicle is passing the host in such a way that the reflections from the centre of the vehicle propagate back towards the radar at an azimuth angle roughly perpendicular to the vehicles heading. The resulting cluster thus seems to be approaching, stationary and moving away at the same time from the radars point of view and a more sophisticated method of determining if the cluster is stationary or not is needed. Since the clustering algorithm has classified all these bin measurements as one object they can be used as input to the velocity and heading estimation described in Section 2.4 and the full velocity vector could instead be calculated.

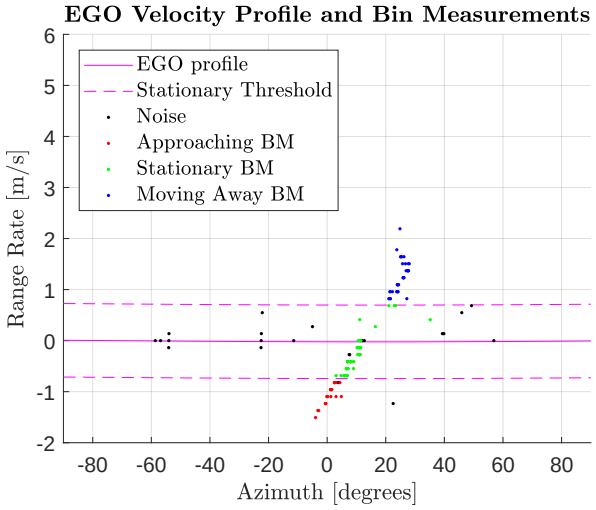

Figure 3.9: Illustration of a scenario where a cluster contains bin measurements that are approaching, moving away and stationary at the same time

3.4.3.1 RANSAC Based Velocity and Heading Estimation

There is always some expected noise when one measures something and this is also true for radar measurements. In addition to the commonly assumed normal distribution with zero mean noise on top of the measurements there are some other noise sources in the radar measurements. Since the doppler measurements are measured in bins rather than a continuous value there is a resolution limitation which can be considered as a noise factor. Furthermore a crude angle finding algorithm is used which brings some additional expected flaws other than the normal distributed

noise with zero mean as is described more in detail in Section 4.1. By taking the noise factors into consideration the bin measurements in a cluster are expected to be very noisy and treating all bin measurements in a cluster equally would result in bad velocity and heading estimations. A widely used method to filter out bad measurements from a set of points used for a regression is RANSAC [8]. RANSAC is an iterative algorithm that randomly takes the minimum number of points needed to solve the desired equation from the data set and then compares how many of the data points are within a certain threshold compared to the current solution. Points within the threshold are called inliers and as the algorithm iterates the number of inliers for the current solution is compared to the solution which had the most inliers so far. If the current solution has more inliers than the one with the most so far the current inliers are stored and the number of them is compared against the inliers from the next iterations. There are many different ways of determining when to stop the iterations. For example one either lets the algorithm run through a fixed number of iterations or stops the iterations once a certain number of inliers are reached. Since the distribution of the bin measurements in a cluster can be very different depending on the distance of the cluster, the orientation and yaw rate of the cluster, the physical size of the cluster etc. a fixed number of RANSAC iterations was used. When the algorithm is stopped the set of best inliers from the iterations are used in a least mean square regression.

4

Results

4.1 Crude Angle Finding

The testing of the performance of the crude angle finding has the issue that the real result or ground truth can never really be known. Even if the exact azimuth of a target is known there is no way of knowing where on the target the reflection comes from and even if it were it is not known how the azimuth spread of the scatter would look like in all surrounding bin measurements. An ideal case could however be staged in a radar chamber where fault sources can be limited and some sort of ground truth is possible by isolating a single scatterer. The result from this test is therefore to be seen as the best possible performance of the algorithm. In a real scenario with multiple scatterers the performance will be degraded.
The walls, floor and ceiling of the chamber is covered with radar absorbing material and the target is a corner reflector. A corner reflector looks like a metallic cone and focuses the radar reflection so that it looks like a point target and therefore makes it possible to control the position of the scatterer. By having the corner reflector centred in the room while rotating the radar it is possible to measure the result of the crude angle finding over different azimuth angles. See Figure 4.1 for a more detailed explanation.

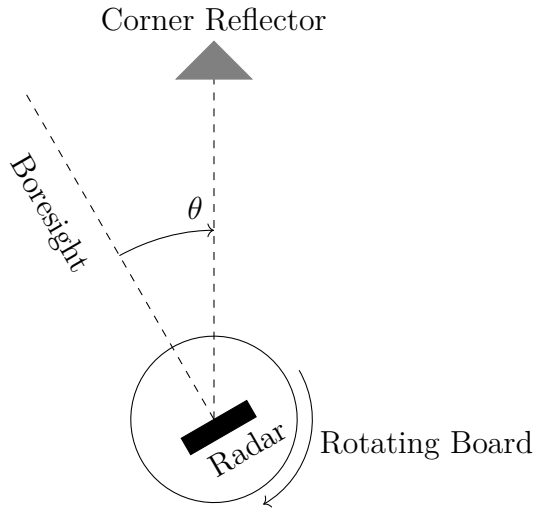

Figure 4.1: Schematic image of the radar chamber setup. A corner reflector is centred in the room and the radar is rotated so that the corner reflector is measured with known azimuth position

The board is rotated with a very precise step motor so that the true azimuth to the corner reflector could be assumed to be exactly known. By comparing the result of the crude angle finding algorithm from each bin measurement with the azimuth of the corner reflector, accuracy over the field of view can be calculated. Figure 4.2 shows a histogram with the absolute value of the crude azimuth error from a sweep between $-75°$ and $75°$. The bin size is $0.25°$ which means that the crude angle finding gives an error that is less than $0.25°$ with 76.69 % probability and less than $1°$ with 96.20 % probability. Noticeable is also that around $22°$, $50°$, $72°$, $96°$ and $125°$ in error there are small group of peaks that in total represents 1.21% probability. This is the result of the algorithm choosing the wrong ambiguous angle from the wide antenna pair as described in Section 3.1.

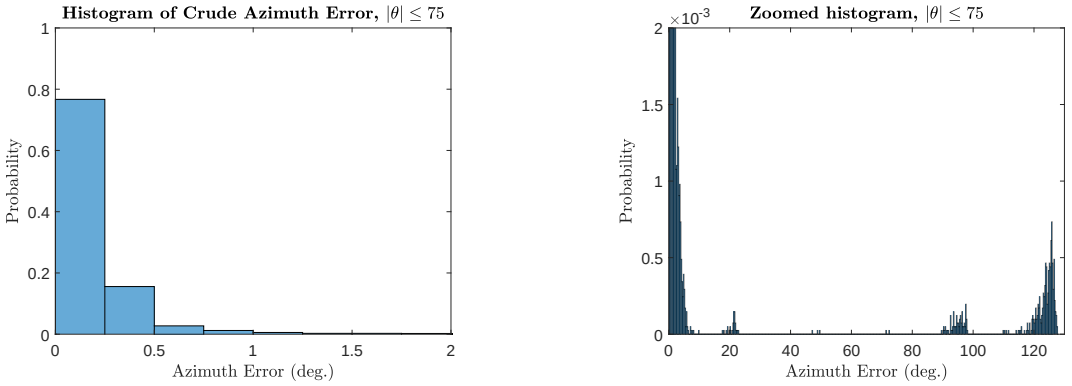

(a) Crude error histogram

(b) Zoomed version to highlight the angle jumps

Figure 4.2: Two histograms describing the absolute error of the crude angle finding algorithm for corner reflector target over the field of view below a magnitude of $75°$. The width of the histogram bars are $0.25°$

If the azimuth lies between $-45°$ and $45°$ the result instead becomes the one in Figure 4.3 where all the measurements is within $1°$ from the true azimuth with a probability of 100 % and no angle jumps occur. This clearly indicates that the crude angle finding algorithm performs worse in the outer edges of the field of view of the radar. If only the outer edges are tested the probability of the $1°$ error is decreased to 90.60 % and the probability of angle jump is increased to 2.98 %. This can be seen in Figure 4.4 where only azimuth angles with a magnitude greater than $45°$ are used in the histogram.

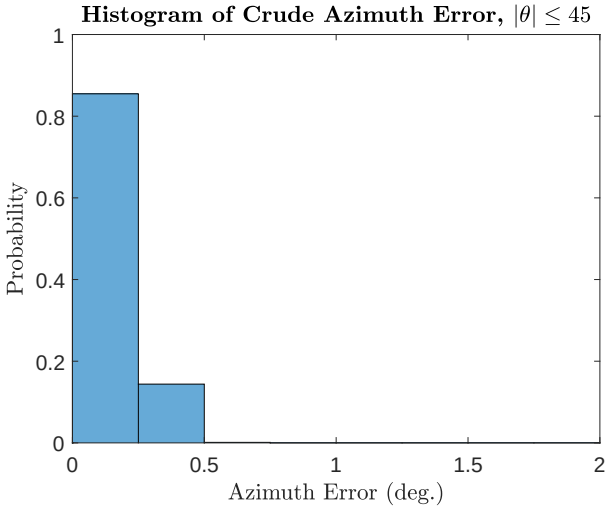

Figure 4.3: A histogram describing the absolute error of the crude angle finding algorithm for corner reflector target over the more narrow field of view below a magnitude of 45°. The width of the histogram bars are 0.25°

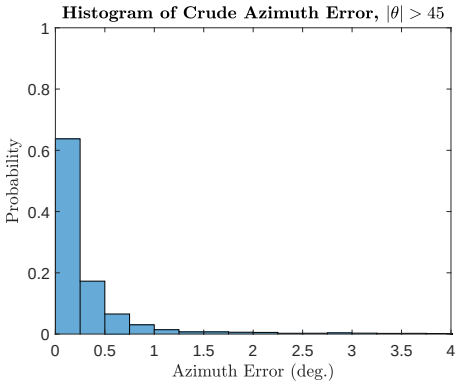

(a) Crude error histogram

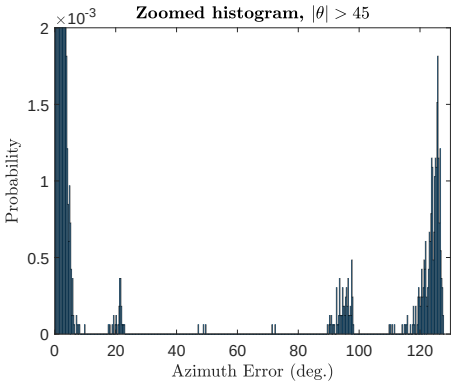

(b) Zoomed version to highlight the angle jumps

Figure 4.4: Histogram of the crude angle finding error for azimuth angles with a magnitude greater than 45°. The width of the histogram bars are 0.25°

The risk of an angle jump as a result of picking the wrong ambiguous angle is a trade-off for having a more accurate azimuth measurement overall. As a comparison, the error of the angle sweep using only the narrow antenna pair is plotted in Figure 4.5. The probability of having an error within 1° is now only 42.47 %.

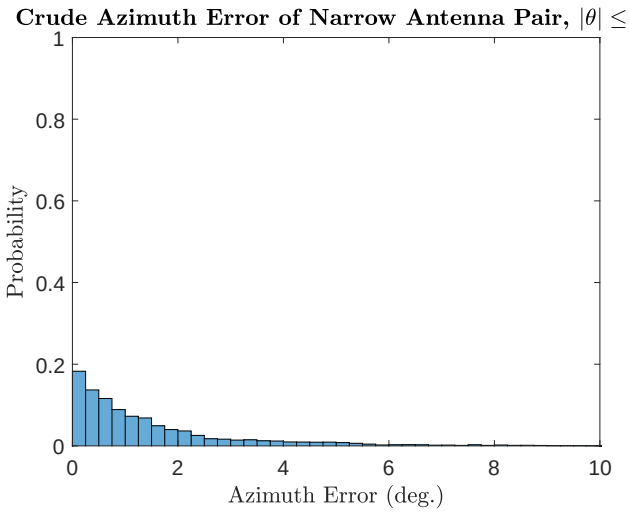

Figure 4.5: Histogram of the crude angle finding error if only the narrow antenna pair is used for azimuth angles below a magnitude of 75°

4.2 Clustering Performance

Also the performance of the clustering algorithm is hard to define with hard values since the desired result may differ depending on the application that should use the data. In this project the most important thing has been to distinguish moving and stationary data and clustering parameters have therefore been tuned to separate bin measurements of moving targets such as cars, bicycles and pedestrians from the rest of the scene. If the goal would have been to distinguish for example guardrails or other stationary objects the clustering parameters would probably be chosen completely different.

In order to see how well the clustering algorithm identifies moving objects it has been run on data from real life traffic scenarios. The advantage of this is of course that the scenarios are more realistic than one from a test track and that the moving targets are surrounded by various stationary targets like guardrails and traffic signs. The disadvantage is however that it was impossible with the equipment available to know exactly the correct position of the objects in the scenario. Below is an example where the radar is mounted on the left side of a truck pointing backwards with a 104° angle from the forward direction of the truck. The truck is driving in the right lane of a two lane highway with a guardrail alongside its left side and is in the same time being overtaken by a car that drives in the left lane. The result of the clustering can be seen in both the range-doppler map and a polar map based on the crude angle in Figure 4.6. Since the car gets scatterers along its side the cluster spreads out in small islands in range, see Figure 4.6b. Cluster centres are calculated with an amplitude weighted average in range as explained in Section 3.4.1 which is the reason why the cluster centres are shifted a little to the left of the average bin measurement location. The data from the car also spreads out in doppler/range rate which is common partly because the measured radial velocity is dependent on the azimuth angle of the scatterer (see Section 2.3), but also because

some scatterers may originate from a spinning wheel which cause a different radial velocity measurement then a scatterer originating from for example the bumper. Even so the clustering algorithm manages to separate the data from the car from the nearest stationary guardrail and by adjusting the parameters it is possible to adjust the kind of separation that is desired. If the neighbourhood is decreased in azimuth the overtaking car now becomes four clusters that marks the front and side of the car, see Figure 4.7. This is probably the result of four or more different scatterers alongside the front and side of the car. Since it has not been a goal for this project to find a perfect combination of cluster parameters that works in all scenarios they therefore have been changed to match the scenario at hand, but with more data from various different scenarios one could of course find a set of parameters that yields a robust result in multiple scenarios.

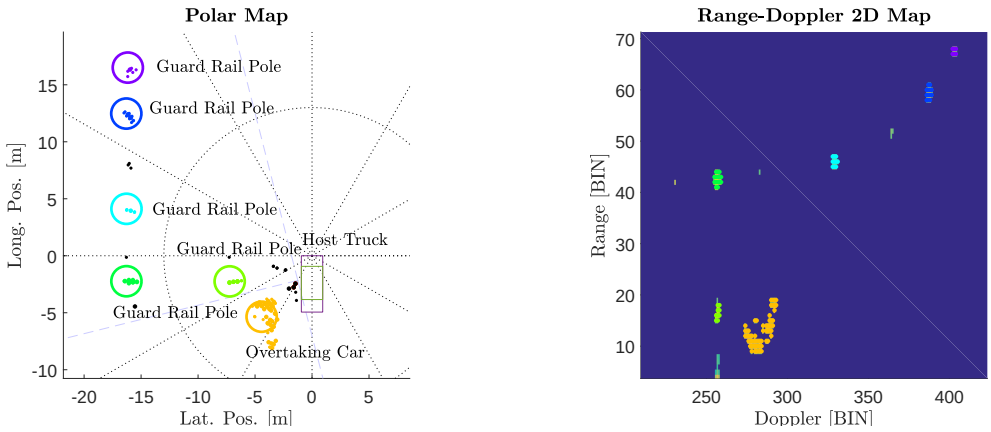

(a) Polar map based on crude angle **(b)** Range-doppler map

Figure 4.6: Range-doppler map and polar map from overtaking scenario. The host moves in positive longitudinal direction and the front of the host is located in origin. The radar is mounted on the left side with boresight pointing backwards with 104° angle from the forward direction. Each cluster is marked with a colour and the overtaking car can be seen as orange. The circles mark the amplitude weighted cluster centres. Two guardrails are visible, the closest ($\sim$ 7 meters left of host) separates the left lane from the oncoming lanes the furthest ($\sim$ 16 meters left of host) marks the side of the road for the oncoming cars

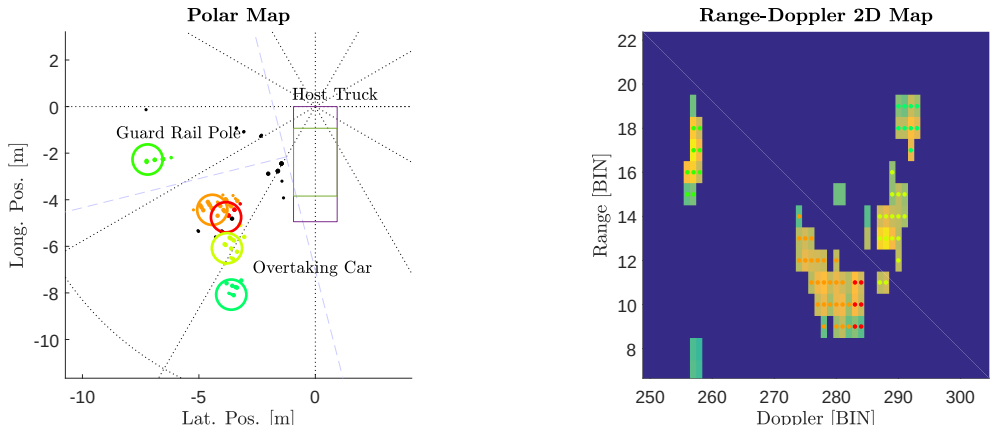

(a) Polar map based on crude angle **(b)** Range-doppler map

Figure 4.7: Range-doppler map and polar map from overtaking scenario. The host moves in positive longitudinal direction and the front of the host is located in origin. The radar is mounted on the left side with boresight pointing backwards with 104° angle from the forward direction. The circles mark the amplitude weighted cluster centres. The overtaking car now consists of four clusters that is spread out alongside the sides of the car and is probably the energy from four different scatter centres

4.2.1 Cluster Properties

The performance of the cluster properties explained in Section 3.4 for the overtaking scenario explained above can be seen in Figure 4.8 where the latitudinal and longitudinal positions are plotted relative to the host truck and the colour of the markers change in every time sample of 100 ms. The host is driving at a speed of approximately 80 km/h and the overtaking car at approximately 93 km/h and the road is straight. It can clearly be seen that the position is very unstable between time samples in the beginning when the car is far away but becomes better and better as it comes closer. This is partly because of errors in range, but especially azimuth has a higher impact on the lateral/longitudinal position when the range increases. The cluster is also located far out in the field of view where the crude angle finding have a bad performance, see Section 4.1, which of course increases the error in azimuth. Moreover are the clusters smaller size since the car only shows its front to the radar and not the side. The position of the car is therefore harder to estimate and is likely to have a cluster centre that is more oriented to the position of the front bumper than a car that shows two sides. The azimuth errors of the bin measurements also have a higher impact on the result when there are fewer bin measurements in the cluster.

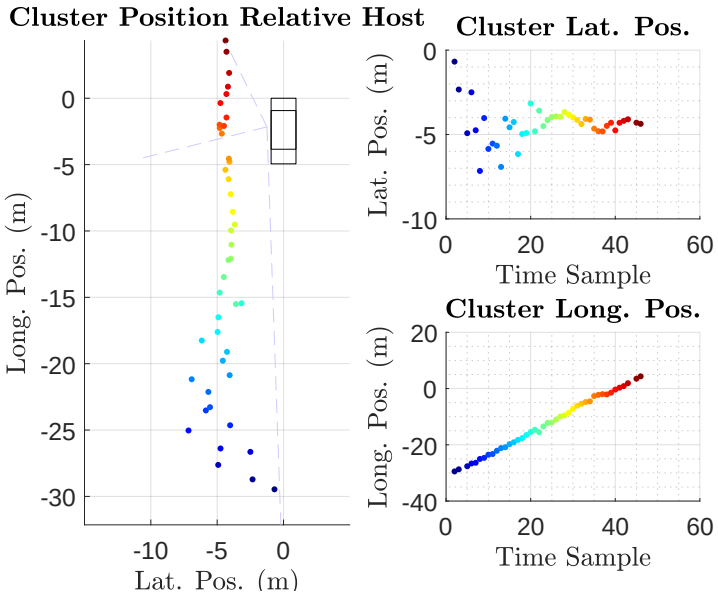

Figure 4.8: Cluster position over time in overtaking scenario. The host truck is overtaken by a car that starts from the right lane, changes lane to the left and drives past host. Time samples are illustrated with colours

4.3 Heading and Velocity Estimation

To evaluate the performance of the velocity and heading estimations certain scenarios were rigged both at an empty parking lot and at a highway where overtaking scenarios were staged. The parking squares were used as a grid to mark out different angles relative to the host vehicle. Two radar units were mounted on a host vehicle as illustrated in Figure 4.12.

4.3.1 Least Square vs RANSAC solution

In Figure 4.9 histograms over the estimated velocity and heading are plotted for all clusters that corresponded to the passing vehicle during one test drive with a known heading and velocity using a simple least mean square solution on all the bin measurements in the cluster. In Figure 4.10 the same scenario and clustered bin measurements are used but the estimated velocity and heading is estimated with a RANSAC solution. As can be seen the RANSAC solution yields a higher probability of estimating the correct velocity and heading. However it also introduces some erroneousness estimations, especially in velocity which the LS solution does not yield which is explained by a low angular spread of the bin measurements in the cluster.

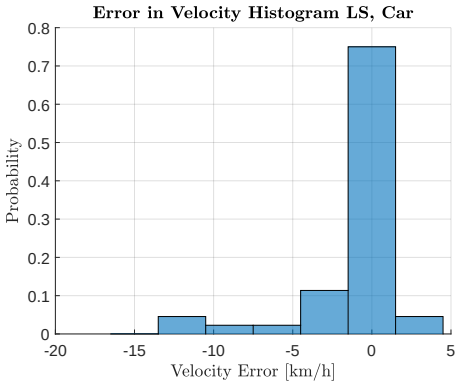

(a) Histogram over the velocity estimations

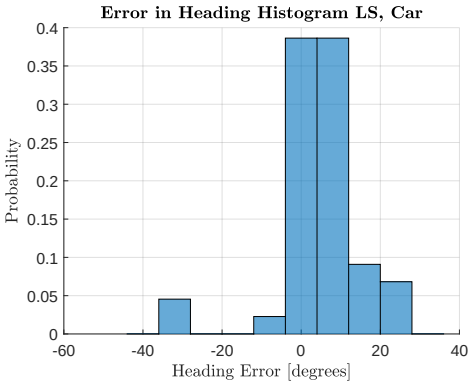

(b) Histogram over the heading estimations

Figure 4.9: Histogram over the error in velocity and heading estimations using a least square solution in a scenario where the target vehicle was following a marked out heading of roughly -155 degrees. The data presented here was collected with the front left mounted radar. The size of the bins used in the histograms is 3 km/h for velocity and 8 degrees for the heading

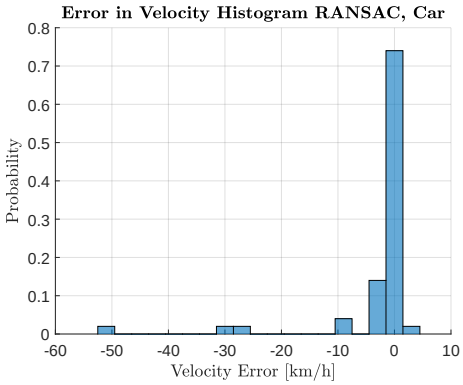

(a) Histogram over the velocity estimations

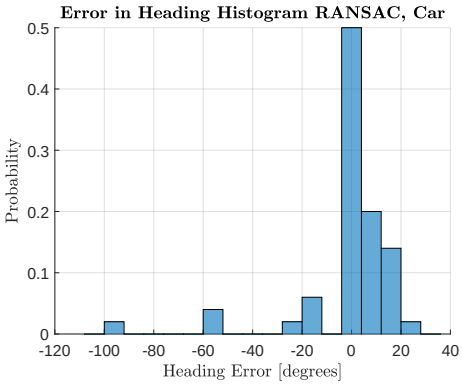

(b) Histogram over the heading estimations

Figure 4.10: Histogram over the error in velocity and heading estimations using a RANSAC solution in a scenario where the target vehicle was following a marked out heading of roughly -155 degrees. The data presented here was collected with the rear left mounted radar. The size of the bins used in the histograms is 3 km/h for velocity and 8 degrees for the heading

Even though there is a distinct peak in the histogram at the true value one can also see that the results are rather noisy and spread out in both the velocity and heading histogram. Since the velocity and heading estimations were done on the clusters without any consideration to the bin measurements they consisted of the spread in estimations is expected. As described in Section 2.4 the velocity and heading estimation is a problem of fitting a cosine curve to the bin measurements in the

cluster and that it is also assumed that several bin measurements from different points on the object are available. If the angle of all the bin measurements in a cluster are close to equal the cluster has no angular spread of the object and the fitting of the cosine curve becomes more or less arbitrary since the bin measurements can be fitted to anywhere on the cosine curve. The RANSAC algorithm yields the solution with the most inliers, however in this case the solution with the most inliers is likely not a good solution. An illustration of the effect a low angular spread has on the cosine fitting problem is presented in Figure 4.11.

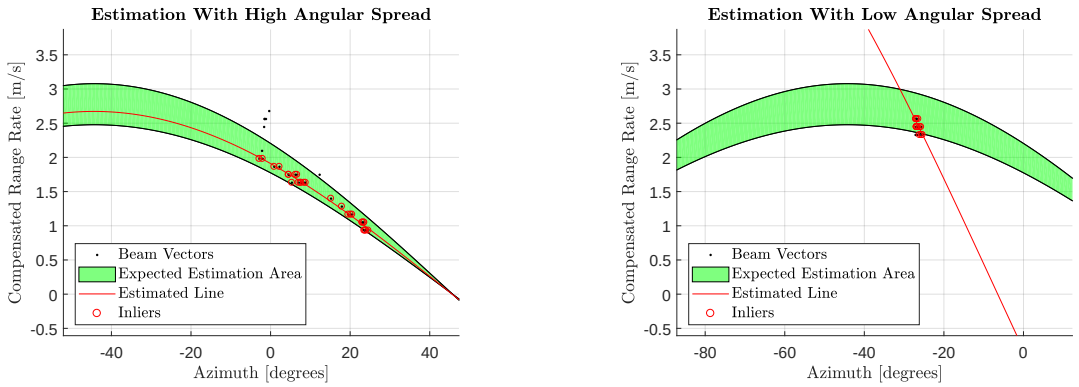

(a) A cluster with a high angular spread

(b) A cluster with a low angular spread

Figure 4.11: A visualisation of the effects that a low angular spread has on the velocity and heading estimation. Since the actual velocity of the car is expected to be around 10 km/h with a heading of roughly -155 degrees an area of the actual velocity profile is plotted in the green area

4.3.2 Arbitrary heading

A reference point was created by parking the host vehicle with the radars on top of a cross between four parking squares. By taking measurements of the dimensions of the parking squares different headings relative to the host could be marked by using a string that intersected corners of the parking squares. Once a heading had been marked a car, a bicycle and a pedestrian travelled along the marked out heading across the field of view. The velocity at which the bicycle and pedestrian travelled was hard to measure but the vehicle was targeted a velocity of 10 km/h. Four different angles relative to the host was marked and the vehicle, bicycle and pedestrian travelled along these marked lines in both direction and thus holding eight different headings relative to the host.

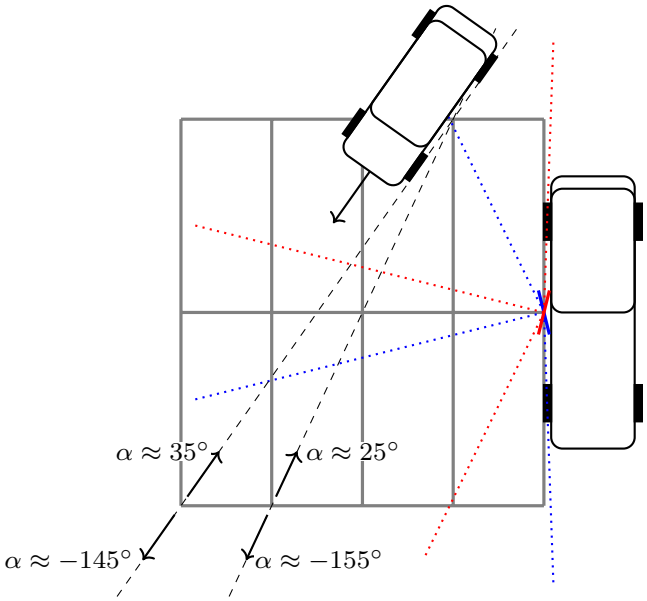

Figure 4.12: Illustration of how the test scenarios were rigged using the parking squares as a grid. A string was then used to mark out trajectories which corresponded to certain headings relative to the host truck. The dashed blue and red lines correspond to the boresight and the field of view of the two radars mounted on the host truck

4.3.2.1 Vehicle

The test vehicle travelled along all the marked out trajectories and the velocity vector estimation was done on the clusters that corresponded to the vehicle. In Figure 4.13 a histogram over the errors in the velocity and heading estimations are presented. An evaluation of how well the velocity and heading algorithm performed depending on the angular spread showed that a minimum angular spread of about 5 degrees is needed for a reasonable estimation to avoid a scenario as in Figure 4.11b. The data sets presented in the histograms in Figure 4.13 have thus been filtered to only contain clusters that have a minimum angular spread of 5 degrees.

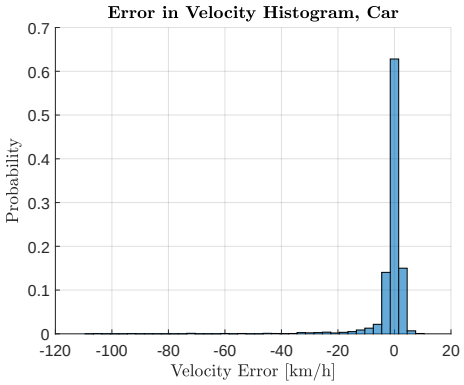

(a) Histogram over the error in velocity estimations of the test vehicle

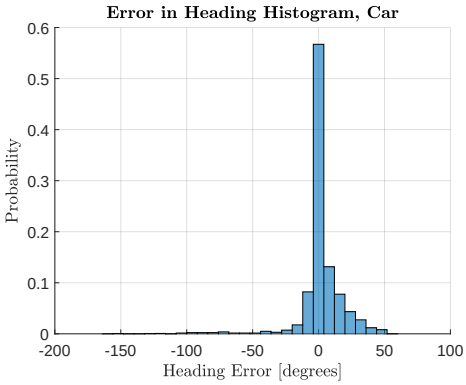

(b) Histogram over the error in heading estimations of the test vehicle

Figure 4.13: Histogram over the errors in the velocity and heading estimations of a vehicle travelling along the marked out trajectories. Clusters with an angular spread less than 5 degrees and a position over 36 meters have been excluded. The velocity bin size is 3 km/h and the heading bin size is 8 degrees. The histograms have been formed using a number of 2627 estimations

4.3.2.2 Bicycle

A bicyclist followed the same marked out trajectories as the vehicle in the previous Section and the velocity vector estimation was done on all the clusters that corresponded to the bicycle. No reference measurement of the bicycles velocity was available but efforts was made to target 10 km/h as this was the targeted velocity for the vehicle in the previous Section. A histogram presenting the performance of the velocity vector estimations of all the trajectories is shown in Figure 4.14 where the same filtering of a minimum angular spread of 5 degrees has been applied as in 4.3.2.1.

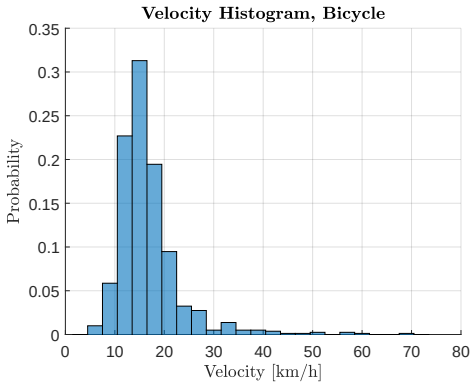

(a) Histogram over the velocity estimations

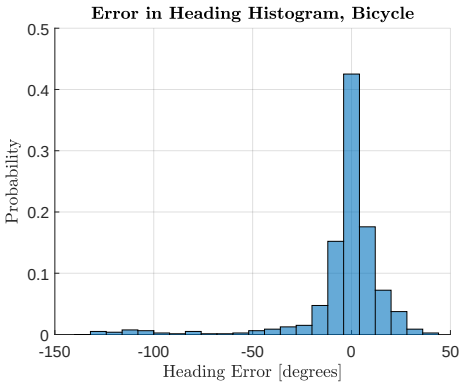

(b) Histogram over the error in the heading estimations

Figure 4.14: Histogram over the velocities and the heading estimations of a bicycle travelling along the marked out trajectories. Note that the estimated velocities are presented rather than the error since no reference measurement of the velocity of the bicycle was available. Clusters with an angular spread less than 5 degrees have been excluded. The velocity bin size is 3 km/h and the heading bin size is 8 degrees. The histograms have been formed using a number of 802 estimations

4.3.2.3 Pedestrian

Data was also collected when a pedestrian walked along the marked out trajectories. However, since the results showed that the velocity vector estimation was not acceptable, a histogram of the error over all trajectories was never created. The result of one trajectory is presented in Figure 4.15 where no filtering of the cluster corresponding to the pedestrian have been applied. No reference measurement of the pedestrian's velocity was available during the data collection.

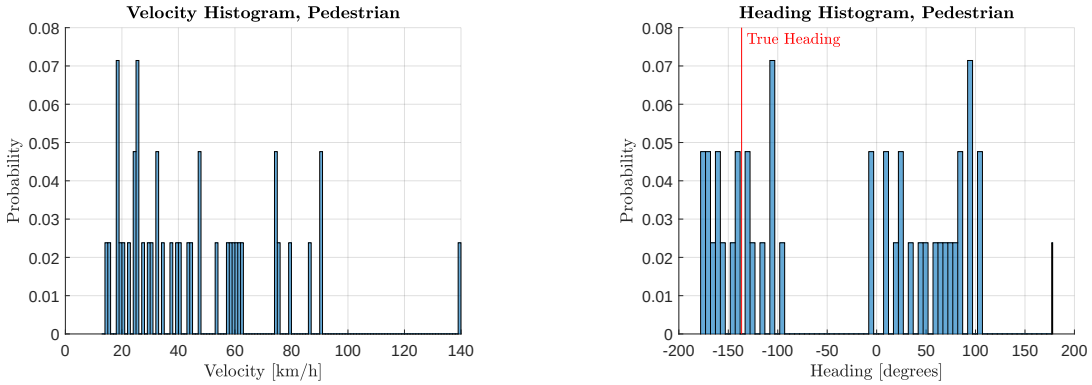

(a) Histogram over the velocity estimations

(b) Histogram over the error in the heading estimations

Figure 4.15: Histogram over the velocity and heading estimations of a pedestrian using a RANSAC solution in a scenario where a pedestrian was following a marked out heading of roughly -136 degrees. The data presented here was collected with the front left mounted radar. The size of the bins used in the histograms is 1 km/h for velocity and 5 degrees for the heading. No actual measurement of the velocity of the pedestrian was available

4.3.3 Overtaking scenario

The data presented in this Section was collected while driving on a highway just outside Gothenburg. The host vehicle was driving in the right most lane while a target vehicle did an overtaking in the left lane of the host. It is the same scenario as presented in 4.2.1 where the position of the cluster was presented. The host held a velocity of 80 km/h using cruise control and the overtaking car aimed to hold a velocity of 93 km/h during the overtaking. However, no cruise control was available in the overtaking car. In Figure 4.16 the estimated velocity vectors are plotted at the longitudinal and latitudinal positions of the cluster during the overtaking. As visible in the Figure 4.16 both the velocity and heading estimations are rather unstable in the first samples where the overtaking car enters the field of view of the radar. As mentioned in 4.2.1 this is partly due to the distance to the object and thus a lower angular spread of the bin measurements in the cluster but also since the overtaking car enters the field of view in an area where the crude angle finding algorithm has bad performance as presented in 4.1. Furthermore the oscillations in the velocity estimations around the targeted value of 93 km/h can partly be explained by the fact that no cruise control was used and that the actual velocity likely deviated some from the targeted velocity. As for the heading it is clear that the best estimations are when the overtaking vehicle is closer to the host and in the more central part of the field of view which yields bin measurements with a good angular spread. It is also visible from the Figure is that the unstable estimations starts to return as the overtaking vehicle approaches the end of the field of view. However, since the vehicle is closer to the radar than when it enters the field of view the cluster consists of several bin measurements which counters the expected degrading performance in the crude angle finding algorithm.

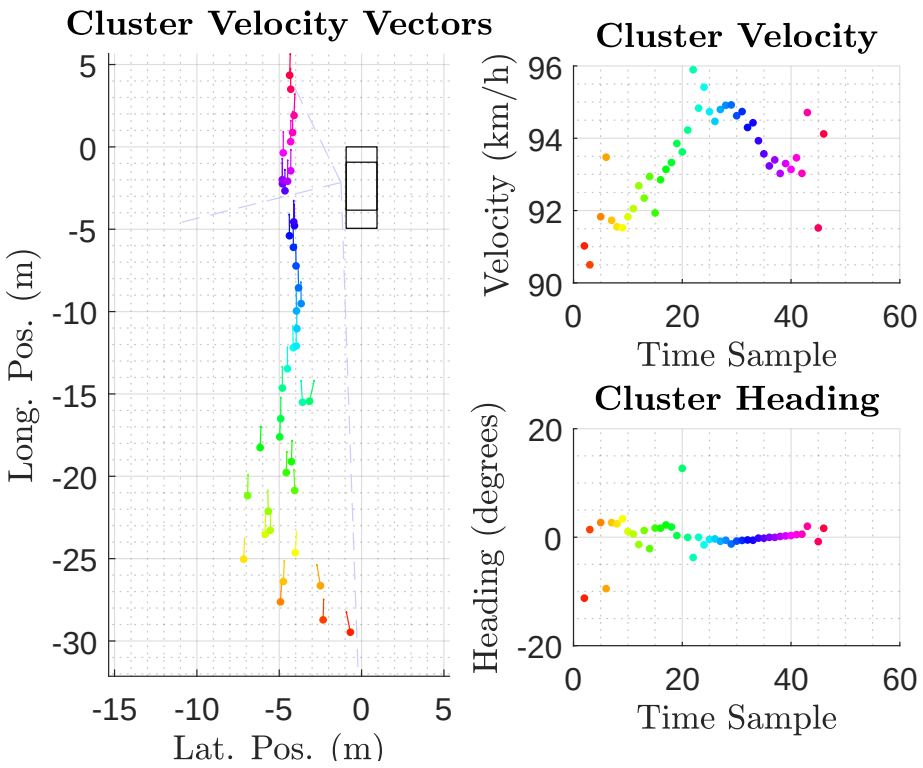

Figure 4.16: The estimated velocity vectors during an overtaking scenario. The host travels at a velocity of 80 km/h using cruise control and the overtaking vehicle targets 93 km/h without cruise control during the overtaking

4.3.4 Vehicles With Considerable Yaw Rate

As described in Section 2.4 the equations that are used to estimate the heading and velocity of a moving vehicle only hold if the motion of the vehicle is linear. If the vehicle is turning with a significant yaw rate the result from the heading and velocity estimation will thus be inaccurate. In this Section a comparison of a simple least squares solution using all the bin measurements in the cluster of the moving vehicle is presented to show the impact on the velocity and heading estimation a strong yaw rate can have. When this data was collected the host was standing still and a vehicle circled the host in a trajectory of an eight on a test track with no other objects or vehicles in the field of view of the radar. At the instant when the data in table 4.1 was collected the circling vehicle was doing a rather strong left turn. For the data presented in table 4.2 the vehicles yaw rate is significantly smaller and the estimation of the velocity and heading is closer to the actual ones.

Table 4.1: Overview of the actual and estimated parameters where the vehicle that the estimation is done for has a considerable yaw rate

	Actual	Estimated	
Velocity	8.5	12.3	[m/s]
Heading	33.3	66.3	[°]
Yaw Rate	27.4	-	[°/s]

Table 4.2: Overview of the actual and estimated parameters where the vehicle that the estimation is done for has a small yaw rate

	Actual	Estimated	
Velocity	9.4	9.6	[m/s]
Heading	56.0	57.8	[°]
Yaw Rate	-3.5	-	[°/s]

5

Discussion

5.1 Crude Angle Finding

The crude angle finding is designed to be what its name suggests, namely a crude angle finding. It is meant to be used as a complement to a more sophisticated angle finding algorithm used to calculate the azimuth of the resulting detections. Thereby it does not have to be perfect. As the results in Section 4.1 show the performance is overall accurate, at least for such an ideal scenario as the angle sweep using a corner reflector in a radar chamber. There are of course some obvious flaws e.g. that it performs a lot worse in the outer edges of the field of view and that there is some risk of angle jumps between the ambiguous angles for the measurement with the wide antenna pair. The use of two antenna pairs introduces as previously mentioned a trade-off between the risk of angle jumps and accuracy. Although the number of angle jumps would probably increase in less ideal scenarios the results from the azimuth sweep with the corner reflector still show that the increase in accuracy is rather high and the risk of ambiguity is quite low. Even if such angle jumps occur, their bin measurements would most probably be considered noise by the clustering algorithm and as long as the target has a considerable amount of other bin measurements that do not result in angle jumps the target would still be captured and analysed with accurate azimuth angles. The negative effects in the host velocity compensation and target velocity estimation from inaccurate azimuth angles if only the narrow antenna pair is used would be a lot more severe. The fact that the angle finding performs badly in the outer edges of the field of view is something that is expected since the $\sin^{-1}$ curve described by Equation (2.1) flattens out in the edges. Small changes in phase difference thereby result in big azimuth changes which makes the result more noise sensitive and inaccurate. The same effect would also affect a more advanced angle finding algorithm since it also depends on the phase to azimuth relationship.

Another disadvantage of the phase comparison monopulse technique is that it cannot handle a signal response that originates from scatterers with similar range and doppler values but with different azimuth. This could potentially be a common scenario in a cluttered environment and would result in phase difference somewhere in between the two incoming signals. The two scatterers would therefore look like one scatter with azimuth somewhere in between. A more sophisticated method like FFT across antennas could handle a spectral distribution of multiple phase differences for the same range-doppler but would be a lot more time consuming [9].

5.2 Clustering and Cluster Position

As explained in Section 4.2 the performance of the clustering is quite hard to evaluate. What is clearly visible however is that the amount of separation of data effectively can be controlled with the parameters of the algorithm and its just a matter of tuning in order to get the result needed for the scenario at hand. Since it has not been a part of the scope to find the perfect parameter set that can function properly with all possible scenarios no real robustness tests have been made but throughout the project the parameters have been held pretty much constant and have not required so much tuning.
One possible improvement however is to implement a scaling of the parameters based on range as the authors of [10], since the neighbourhood size in azimuth dramatically increases with range. An object that is close to the radar thereby has a higher spread in azimuth than an object that is far away. This makes the clustering less restrictive at high ranges than at closer range and the risk is that objects far away are grouped together or that close targets are grouped into multiple clusters. This did not cause any problems in the scenarios investigated in this project but might be in more cluttered scenarios with a lot of moving objects close to each other.
The calculation of cluster positions also has potential of improvement since it is a rather simple solution that was designed to work for multiple types of objects with different shapes without making any assumptions of how a target might look like. The position is mainly used to determine the importance of the data in the range-doppler map. It is not needed for the target velocity estimation and the tolerance of the error in position is therefore high. A more accurate solution might be to estimate the edges of the target and with that information determine the mass centre of the geometric shape. If the cluster could be identified as a specific class of object, like car, bicycle or guardrail, one could also have a more advanced model of where the centre should be based on the edges.

5.3 Velocity and Heading Estimation

In Figure 4.9 and 4.10 a comparison of the LS and RANSAC solution using the same data is presented. As can be seen the RANSAC solution yields a higher probability of estimating the correct velocity and heading compared to the LS. However the RANSAC solution yields some erroneous estimation that the LS solution does not. Since the RANSAC solution only uses points that are inliers to perform the regression it is possible that there is no solution to which many of the bin measurements are considered inliers. This causes the RANSAC solution to output the solution which indeed holds the most inliers but the inliers used in the regression have a low angular spread which in turn causes an erroneous estimation as is presented in Figure 4.11. The LS solution is more robust against these situations since all bin measurements in the cluster are used in the regression. However by using all the bin measurements in the cluster, which in general are rather noisy, the LS solution has the downside of an overall decreased accuracy in the estimations compared to the RANSAC solution.

The problem of estimating the velocity vector of an object is a problem of fitting a cosine curve to the bin measurements in the cluster corresponding to the object. As stated in Section 2.4 it is necessary that multiple points of the object is observed by the radar since the theory is derived based on the fact that the range rate vectors of a moving object are different based on where on the object they are measured. Since the bin measurements in the clusters are rather noisy it is crucial that the bin measurements have a large angular spread of the object for the velocity vector estimation to yield descent results. In Figure 4.11 a visualisation of how the estimation is effected when the cluster has a high angular spread versus a cluster with low angular spread. The angular spread of a cluster corresponding to an object is dependent on its physical size and the orientation and the distance of the object relative to the radar. Other objects that are located in between the radar and the object and thus block parts of it also lead to a low angular spread. By analysing many scenarios it was found that a minimum angular spread of 5 degrees was generally needed for the velocity vector estimation to yield acceptable results. Depending on whether the physical size and orientation of the object relative the radar the minimum angular spread can be translated to a maximum distance from the radar where the velocity vector estimation is possible. Assuming that an average car is 1.7 meters wide and 4.5 meters long and that a bicycle is 1.5 meters long and when it comes to the observed width of a bicycle the person riding defines the width. An average person is assumed to be 0.6 meters wide. The table presented in 5.1 is supposed to give a rough approximation to the maximum distance when the velocity vector estimation is possible given an assumed minimal angular spread of 5 degrees.

Type	Car		Bicycle	
Orientation	Front/Back	Side	Front/Back	Side
Max Distance [m]	19.5	51.5	6.9	17.0

Table 5.1: Maximum distance of an object where the velocity vector estimation is possible given a minimal angular spread of 5 degrees of the object. The assumed dimensions of a car is in this case 4.5 meters long and 1.7 meters wide. The observed area of a bicyclist is assumed to be 1.5 meters in length and 0.6 meters in width. Note that these are rough estimates to give an approximation to the the maximum distance where velocity vector estimation is possible

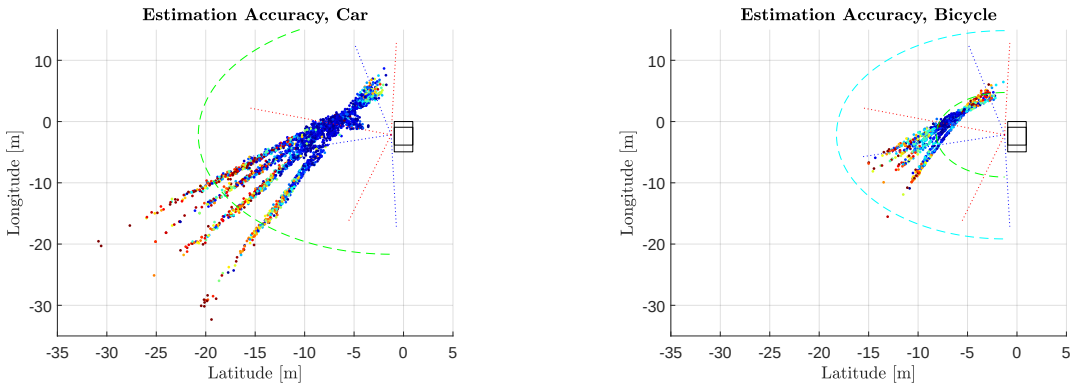

(a) Estimation Error Car

(b) Estimation Error Bike

Figure 5.1: The accuracy of the velocity vector estimation decreases with increasing distance to the object. Blue points are cluster position with a low error in the velocity vector estimation while red points are cluster positions with a high error in velocity estimation. The dashed green and cyan lines are the radius of the roughly estimated maximum distance to an object where velocity vector estimations are possible presented in table 5.1

The velocity vector estimation of a pedestrian did not yield accurate results. This can partly be explained by the fact that the relative small dimensions of a person inevitably results in a low angular spread observed by the radar. However the width of a person resulted in a sufficient angular spread when a person was riding a bicycle. It is important to note that the radar measures the radial velocity of whatever its transmitted wave reflects on. This means that the velocity measurements from a pedestrian can result in many different velocities depending on the transmitted wave was reflected on the person's leg, arm or upper body. In general, as a person moves one leg is stationary while the other leg moves forward as the person takes the next step. Furthermore the person often swings the arms along with the steps and the upper body moves more or less in a smooth linear motion. This breaks the assumption stated in Section 2.4 that the object moves in a linear motion and it is thus expected that the velocity vector estimation should not work. For a bicyclist the upper body along with the arms move in a linear motion along with the frame of the bicycle. As the person is pedalling the legs do move and thus breaks the assumption of a linear motion. However, since the motion from pedalling is a motion of moving the legs up and down rather than back and forth no radial velocity is detected by the radar as this motion is perpendicular to the transmitted wave. Since most of the movement of the legs are not measured by the radar the assumption of a linear motion still holds and velocity vector estimation should be possible.

5.4 Future Work

As mentioned earlier a suitable improvement would be to implement a clustering that is range dependent in the way that the neighbourhood changes size over range. By keeping the neighbourhood constant on all ranges the risk of splitting big targets

at close range and grouping far targets together is decreased. General clustering parameters that produce a robust result in multiple different scenarios could also be found with more test driving. This will be needed if the clustering and velocity vector estimation is to be tested online in a car.
Regarding the velocity vector estimation the performance should be more accurate if the clustered bin measurements from multiple radars are fused together as this would increase the number of bin measurements of an object. If the radars are mounted on different locations on the host but still covers the same or parts of the same field of view an increased angular spread of the object is available and the velocity vector estimation should thus yield more accurate results. This would though require that all the clustered data gets passed to some CPU or a radar master unit where the measurements are being transformed to the same reference system and then a velocity vector estimation is possible. Another possible way to increase the accuracy of the velocity vector estimation is to use some weighing scheme of the bin measurements amplitude when counting inliers in the RANSAC solution. This idea is based on the fact that a peak in magnitude in the range doppler map indicates a strong reflection from an object and the bin measurement with a high amplitude should thus be considered as a more valuable measurement.
The velocity vector of an object could be used higher up in the signal processing chain where a tracker could benefit from instantaneous estimations of an objects velocity and heading. The object could be tracked over time where the deviations from the correct velocity vector could be countered using a well-tuned Kalman filter that models the objects movement using a for example a constant velocity model.
Lastly could future work also be to implement the full system with crude angle finding, clustering and velocity vector estimation together with the detections prioritisation online in a car. The clustering and velocity of targets would here benefit both the prioritisation of detections but also enables that detections could be reported as groups belonging to the same target, but each detection would also have an instantaneous velocity vector.

6
Conclusion

The results presented in this thesis show that it is possible to use a crude angle finding algorithm on all the bin measurements in the range doppler map with satisfactory results given that no mixing of reflections from multiple objects at similar range occurs. Furthermore it has been shown that it is possible to use the crude angle estimation along with the corresponding range and doppler bin pair to cluster bin measurements in a range doppler map using a grid based DBSCAN technique. Even though no fixed clustering parameters have been presented that would properly cluster targets independent of type and direction such as guard rails and oncoming/parallel travelling cars or bicycles at all ranges, an improvement to use adaptive clustering parameters has been suggested. Furthermore the lateral and longitudinal position of clusters are calculated using an amplitude weighing technique which showed to be rather accurate as presented in Section 4.2.1. Using the bin measurements in a cluster corresponding to a moving object a velocity vector estimation has been developed which yielded acceptable results given a minimal angular spread of the object as presented in 4.3.2.

Bibliography

[1] Tom Jeffrey, IET Digital Library (e-book collection), Books24x7 (e-book collection), Knovel (e-book collection), and Inc Books24x7. *Phased-array radar design: application of radar fundamentals*. SciTech Pub, Raleigh, NC, illustrat edition, 2009;2013;.

[2] David K. Cheng. *Field and wave electromagnetics*. Pearson, Harlow, Essex, England, 2nd, pearson new international edition, 2014.

[3] Dominik Kellner, Michael Barjenbruch, Jens Klappstein, Jurgen Dickmann, and Klaus Dietmayer. Instantaneous ego-motion estimation using doppler radar. In *Intelligent Transportation Systems-(ITSC), 2013 16th International IEEE Conference on*, pages 869–874. IEEE, 2013.

[4] Vehicle Dynamics Standards Committee. Vehicle dynamics terminology. Standard, SAE International, Warrendale, PA, USA, January 2008.

[5] Lennart Råde and Bertil Westergren. *Beta: mathematics handbook : concepts, theorems, methods, algorithms, formulas, graphs, tables*. Studentlitteratur, Lund;Bromley;, 1988.

[6] Dominik Kellner, Michael Barjenbruch, Jens Klappstein, Jurgen Dickmann, and Klaus Dietmayer. Instantaneous ego-motion estimation using doppler radar. In *Intelligent Transportation Systems-(ITSC), 2013 16th International IEEE Conference on*, pages 869–874. IEEE, 2013.

[7] Martin Ester, Hans-Peter Kriegel, Jörg Sander, Xiaowei Xu, et al. A density-based algorithm for discovering clusters in large spatial databases with noise. In *Kdd*, volume 96, pages 226–231, 1996.

[8] Martin A. Fischler and Robert C. Bolles. Random sample consensus: A paradigm for model fitting with applications to image analysis and automated cartography. *Commun. ACM*, 24(6):381–395, June 1981.

[9] Stephan V Schell and William A Gardner. 18 high-resolution direction finding. *Handbook of statistics*, 10:755–817, 1993.

[10] Dominik Kellner, Jens Klappstein, and Klaus Dietmayer. Grid-based dbscan for clustering extended objects in radar data. In *Intelligent Vehicles Symposium (IV), 2012 IEEE*, pages 365–370. IEEE, 2012.

A

Appendix 1

A.1 DBSCAN Pseudo Code

Below is a pseudo code representation of how the DBSCAN was implemented on the range-doppler-azimuth map from the crude angle finding. *azimuthMap* is the range-doppler-azimuth map, *eps* is a vector describing the neighbourhood of a point, *minPts* is the amount of neighbours a point must have in order for the density to be high enough, *clusterID* is a map with the IDs for every point in the range-doppler-azimuth map, *typeOfPoint* is a similar map describing what kind of points the clustered points are. Core points is marked as 1, border points as 2 and noise as 0.

Input: azimuthMap, eps, minPts
Output: clusterID, typeOfPoint

```
points := find a list of indices in the azimuthMap that contain nonempty values
nbrOfPoints := the number of nonempty points found

clusterID := empty map of cluster ID:s (same size as the azimuth map)
typeOfPoint := empty map point types (same size as the azimuth map)

currentClusterID := 0
for all p in points do
    if typeOfPoint[p] is not empty then
        skip iteration % This point is already clustered
    end if

    n := rangeQuery(azimuithMap, p, eps);
    nbrOfNeighbours := length of n

    if nbrOfNeighbours < minPts then
        typeOfPoint[p] := 0 % This point is noise
        continue with next iteration
    end if

    % Make new cluster and assign core point to p
    currentClusterID += 1
    clusterID[p] := currentClusterID
```

```
19:     typeOfPoint[p] := 1

20:     while n is not empty do
21:         % If point is noise make it a border point
22:         if typefPoint[n[1]] == 0 then
23:             clusterID[n[1]] := currentClusterID
24:             typeOfPoint[n[1]] := 2
25:             remove n[1] from n
26:             continue with next iteration
27:         end if

28:         % If point is already clustered remove it from list
29:         if typeOfPoint[n[1]] is not empty then
30:             remove n[1] from n
31:             continue with next iteration
32:         end if

33:         % Assign point to cluster and get its neighbours
34:         clusterID[n[1]] := currentClusterID
35:         nn := rangeQuery(azimuthMap, n[1], eps)

36:         % If density around the point is high enough make it a core point
37:         if nn is longer than minPts then
38:             typeOfPoint[n[1]] := 1
39:             remove n[1] from n
40:             n := n ∪ nn
41:         else% Else make it a border point
42:             typeOfPoint[n[1]] := 2
43:             remove n[1] from n
44:         end if
45:     end while
46: end for

47: function RANGEQUERY(azimuthMap, pointIndex, eps)
48:     rangeBin := calculate range bin from pointIndex
49:     dopplerBin := calculate doppler bin from pointIndex
50:     azimuth := azimuthMap[pointIndex]

51:     p := all points in azimuthMap within rangeBin ± eps[1] and dopplerBin ±
    eps[2]
52:     n := all nonempty points in p that are |azimuthMap[p]-azimuthMap[pointIndex]|<eps[3]
53: end function
```